EFFECT OF LIQUID TRANSPARENCY ON LASER-INDUCED MOTION OF DROPS

By

ROHIT SHUKLA

Bachelor of Science in Mechanical Engineering

Mumbai University

Mumbai, Maharashtra

2005

Submitted to the Faculty of the
Graduate College of the
Oklahoma State University
in partial fulfillment of
the requirements for
the Degree of
MASTER OF SCIENCE
December, 2007

EFFECT OF LIQUID TRANSPARENCY ON LASER-INDUCED MOTION OF DROPS

Thesis Approved:

Dr. K. A. Sallam
Thesis Adviser

Dr. F. W. Chambers

Dr. A. J. Ghajar

Dr. A. Gordon Emslie
Dean of the Graduate College

ACKNOWLEGDEMENTS

I would like to thank Dr. K. A. Sallam for his support and guidance on this thesis. I am also grateful to Dr. F. W. Chambers and Dr. A. J. Ghajar for their participation on the thesis committee.

TABLE OF CONTENTS

LIST OF TABLES

LIST OF FIGURES

NOMENCLATURE

Alphabetical

a = Absorptance

A_h = Surface area of heated region, m^2

ΔA_h = Change in surface area of heated region after heating, m^2

A_l = Cross-sectional Area of laser, m^2

A_s = Area of the spark, m^2

c = Specific heat capacity of water, 4200 J/kgK

c_a = Absorption coefficient, m^{-1}

d = Diameter of the drop, m

E_a = Flux absorbed, W/m^2

E_e = Flux emitted, W/m^2

E_i = Incident laser flux, W/m^2

E_{losses} = Flux lost from the spark, W/m^2

E_{spark} = Flux absorbed from the spark, W/m^2

E_t = Energy transmitted through the drop, J

f = Focal length of the drop ball lens, m

f_l = Fraction of the drop in physical contact with the substrate

F = Tensiometer correction factor

F_{act} = Actuating force on the drop for the motion, N

F_{aero} = Aerodynamic drag on the drop, N

F_{sres} = Surface resistive force on the drop, N

F_{net} = Net force acting on the drop (F_{act}- F_{aero} - F_{res}), N

F_{res} = Total resisting force on the drop (F_{aero} + F_{res}), N

F_{RP} = Force due to Radiation Pressure, N

H = Diameter of the laser, m

KE = Kinetic Energy of the drop, J

L = Pathlength, m

lp = Drop geometry (length used in the code), m

m = Mass of the heated region of the drop, kg

n = Number of cells penetrated by the laser beam

p = Apparent surface tension, mN/m

P = Laser power, W

r = Radius of the spherical cap that the laser beam heats, m

R = Radius of the drop, m

ΔR = Increase in drop radius at the heated region, m

s = Distance traveled, m

S =Actual surface tension, mN/m

SE = Surface Energy change, J

T_1 = Ambient Temperature, K

T_2 = Raised temperature of the drop, K

ΔT = Change in temperature (T_2-T_1), K

T_s = Temperature of the spark, K

u = Drop velocity, m/s

v = Heated volume, m^3

Δv = Change in the heated volume, m^3

w = Surface contact diameter, m

x = Sector length (maximum pathlength, code), m

y_n = Height of each cell (code), m

z = Diameter of heated region for opaque drop from drop geometry, m

Greek

α = Absorbance

β = Thermal expansion coefficient of water, $0.3E\text{-}3m^{-3}$

γ = Drop geometry angles (code), degrees

δ = Drop geometry angles (code), degrees

ε = Emissivity of the drop

ϕ = Angle of drop motion, degrees

θ_A = Advancing contact angle, degrees

θ_R = Receding contact angle, degrees

μ = Refractive index of the drop liquid

μ_0 = Viscosity of air, Ns/m^2

μ_i = Viscosity of water, Ns/m^2

ξ = Angle between the drop motion and the horizontal, degrees

ρ = Density of air, kg/m^3

σ_c = Higher surface tension at ambient temperature (cold), N/m

σ_h = Lower surface tension at elevated temperature (hot), N/m

$\Delta\sigma$ = Change in surface tension of the drop ($\tau_h - \tau_l$), N/m

υ = Speed of light, m/s

ψ = Drop geometry angles (code), degrees

ω = Angle between beam and horizontal, degrees

ABSTRACT

An Experimental investigation of the role of liquid transparency in controlling laser-induced-motion of liquid drops is carried out. Droplets with diameters of 1–4 mm were propelled on a hydrophobic substrate using pulsed-laser beam (532 nm, 10 Hz, 3-12 mJ/pulse) with 0.9 mm diameter fired parallel to the substrate. The test liquid was distilled water whose transparency was varied by adding different concentration of Rhodamine 6G fluorescent dye. Motion of the drops was observed under a camera. Measurements include direction of motion, distance traveled before the drops come to rest, and drop acceleration at the start of the motion. The motion of both transparent and opaque drops was dominated by thermal Marangoni effect. The present results show that direction of motion depends on the drop transparency; opaque drops moved away from the laser beam, whereas transparent drops moved at small angles toward the laser beam. This is plausible because the laser beam was absorbed near the front face of opaque drops, whereas the laser beam was focused near the rear face of transparent drops. Energies lower than 3 mJ were incapable of moving the drops and energies higher than 12 mJ shattered the drops instead of moving them. The distance the drops move follows a log-normal profile, with most of the drops moving about 5 drop diameters. A phenomenological model is developed for the drop motion which explains the physics behind the phenomenon. The entire process of drop motion has the potential of being automated.

CHAPTER I

INTRODUCTION

1.1 Background

Manipulation of liquid drops over a substrate has a wide range of applicability, especially in microfluidics. Channel-based microfluidics has dominated much of the research and development in this field, an alternative approach to conventional channel-based microfluidics is the use of discrete liquid drops to perform fluidic operations. In the field of microfluidics, droplet based techniques offer an efficient fluid manipulation mechanism, a key to successful microfluidic devices for bio and chemical applications. In channel-based techniques, whole bulk of fluid is moved around in channels especially manufactured for this purpose, usually through lithography. Although there have been advances in these techniques and manufacturing channels on a substrate is easier now, many of the initial drawbacks including the need to manufacture micro-pumps, valves, mixing channels and sometimes bubble chambers are still present.

Since surface forces dominate at the microscale, a technique that utilizes surface forces is an efficient one for fluid transport at the microscale. Droplet motion actuated by surface forces is thus a suitable method for fluid manipulation at the microscale. This approach allows the use of very small quantities of samples and reagents, for bio-chemical analysis (Kotz et al., 2005) such as High-Throughput Screening (HTS),

combinatorial chemistry, DNA sequencing, cell separation and detection, with the potential to replace an entire lab with a droplet-based lab-on-a-chip, paving the way forward for new methods in bio-chemical research. Droplet-based techniques also offer several other advantages over channel-based techniques, such as simple substrates, no electrical connections, no moving parts and better fault tolerance. Drops can also be used as the digital equivalent of microelectronics for constructing basic microfluidic logic gates (AND/OR/NOT) as shown by (Cheow et al., 2007).

Application of lasers in droplet-based microfluidics is contemporary, however, the effect of laser radiation on drops is not new and was a hot topic of research during the Cold War years. Remote sensing of the atmosphere being a major propellant for such research, amongst others. In USSR the impetus being led for the propagation of laser radiation through water aerosol (Bisyarin et al., 1983), heating of water droplets by laser (Prishivalko and Leiko, 1984) and finally the explosion of drops under intense laser radiation (Zuev and Zemlyanov, 1983). The effect of laser on opaque drops was also studied (Ivanov et al., 1977). In USA too, the explosion of water drops under laser was studied (Singh and Knight, 1978; (Carls and Brock, 1987), so was the process of droplet heating under a continuous laser beam (Park and Armstrong, 1989) and also the hydrodynamics of a drop when exposed to pulsed laser (Zardecki and Pendleton, 1989). (Autric et al., 1988) also reported their findings on the effects of pulsed CO_2 on water droplets. The focus of the study of atmospheric laser propagation has also included cloud science, particularly cloud-clearing using high-energy laser beams and new applications such as wireless communication using laser beams.

The laser-induced spark observed in the present study was applied for internal combustion engines (Phuoc, 2006) where it offers various benefits over the conventional spark plug and can potentially replace it.

This study investigates the effect of drop transparency on laser-induced drop motion on a solid hydrophobic substrate using a pulsed Nd:YAG laser beam. Thermal Marangoni effects induced by the laser beam are used for moving the drops.

1.2 Problem Statement

Surface tension forces dominate inertial forces at small scale, thus a method to manipulate drops using surface tension forces is desired. A hydrophobic substrate is required for the production of drops on it and a technique needs to be developed for the subsequent motion of the drops on the hydrophobic substrate. These results are of interest to the field of microfluidics since they provide a low cost substitute for lab-on-a-chip devices. The effect of drop transparency on laser propagation is desired to be known which has not been investigated earlier. Also, the properties of the laser-induced spark need to be examined.

1.3 Previous Studies

Several attempts have been made at droplet manipulation for various applications, primarily bio-chemical research. The numerous ways by which droplets can be moved on a substrate are - Droplet manipulation via the thermal Marangoni Effect: Surface tension and surface energy generally drop as temperature is increased. If a thermal gradient is applied along a droplet, the droplet moves toward the colder region to minimize the total

surface energy, this effect is called the thermal Marangoni effect. This effect has been demonstrated by many researchers as follows: (Grigoriev et al., 2006) who showed mixing in a drop on a liquid substrate by breaking flow invariants and chaotic advection, as shown in Fig. 1.1. Mixing on fusion by dissipation of kinetic energies of the drops in the form of viscous dissipation (Kotz et al., 2004), water drops immersed in decanol were employed in this study, the experimental set up used for this study is shown in Fig. 1.2 (1) and their results are shown in Fig. 1.2 (2). A heated grid of thin metal lines has also been used to move drops (Farahi et al., 2004) across the grid in one dimension by the thermal Marangoni effect by varying the temperature of the metal lines on the grid. The drop moves toward the colder lines. Analytically also demonstrated by (Ford and Nadim, 1994). Manipulation of large oil (nitrobenzene) droplets in a liquid (water) substrate using continuous wave 532nm laser (Rybalko et al., 2004). They showed that the direction of translation of the drop can be changed by changing the optical path of the laser through the drop. The drop moves toward the laser beam when the laser beam is introduced at the oil-air interface and away from the laser when introduced at the bottom of the drop within the water substrate as shown in Fig. 1.3. Translation here is a result of the convection within the drop.

Droplet manipulation on a substrate with a wettability gradient, the drops move from a region of hydrophobic substrate to a region which is more hydrophilic as demonstrated by (Yang et al., 2004; (Moumen, 2006). Another technique known to exist for changing the wettability is by surface morphology change (Chen et al., 2007).

Spontaneous motion of a drop due to surface tension gradients created by oxidation-reduction reactions (Kitahata, 2006) within the drop has been reported on the

much larger question of the existence of living organisms. The drop moves in the direction of the oxidation reaction where the surface tension is more. Electric field gradient induced surface tension imbalances (Cho et al., 2003) have been used to move drops, so have been used light forces for fluidic control using photoisomerization to change surface energy by photoirradiation of a photoresponsive substrate causing a surface energy gradient (Oh et al., 2000). Droplet manipulation via excitation of surface plasmons (Farahi et al., 2006), whose decay in turn causes a flow of microdrops for physical-, chemical- and bio-sensing applications. The surface plasmons produced from the surface are made to travel in the direction of the drops, where they push the drops to cause motion.

Radiation pressure forces (optical traps and optical tweezers) can be used to move relatively small drops. Optical trapping (Ashkin, 1987) has been an enabling factor behind investigations into the interaction of light and matter on the micron and smaller scales. Optical tweezers (Dholakia et al., 2002) work because transparent particles with a higher index of refraction than their surrounding medium are attracted towards the region of maximum laser intensity. By moving the focus of the beam around, it is therefore possible to transport the particle. Indeed, with optical tweezers it is possible to grab and move dielectric objects and biological samples – ranging in size from 100's of nanometers to 10's of microns. Although the optical forces might only be of the order of piconewtons, such forces can often be dominant at the micro-level. A system for driving fluid in microchannels using an optically driven pump which relies on optical trapping has been reported by (Mushfique et al., 2006). This consisted of two optically trapped rotating particles, whose rotation causes a flow in between them.

Electrowetting-on-dielectric (EWOD) (Fowler et al., 2002; (Cho et al., 2003) is another method for moving drops. In this method the drops are squeezed between two plates and moved around by the application of electric field on the plates. Droplet formation in microchannels has also been demonstrated (Ozen et al., 2006) and their manipulation (Song et al., 2006), in which droplets act as small reactions chambers. Electric field gradient through Dielectrophoresis is a mode for drop transportation too. Dielectrophoresis is the motion of polarizable particles that are suspended in an electrolyte and subjected to a spatially nonuniform electric field (Karniakadis et al., 2001). The particle motion is produced by the dipole moments induced on the particle and the suspending fluid due to the nonuniform electric field. When the induced dipole moment on the particles is larger than that of the fluid, the particles move toward regions of high electric field density. This is known as Dielectrophoresis and has been employed to move drops on a chip (Velev et al., 2003) as shown schematically in Fig. 1.4. In the case of the fluid being more polarizable than the particles, the particles move away from the high electric field density, which is known as Negative-Dielectrophoresis. Motion of drops on a solid surface using acoustic radiation pressure was shown by (Alzuaga et al., 2005). They migrated a drop on a vibrating beam, toward the anti-node of the vibration. Other work in this field includes the motion of a phase separated fluid under the influence of laser light scattering of density fluctuations (Scroll et al., 2007) within the liquid. Laser-induced motion in nanoparticle suspension droplets spreading on a flat surface was investigated numerically by (Dietzel and Poulikakos, 2005). The spreading of microscale liquid films on solid substrates and liquid flow manipulation on a surface using optical perturbations (Garnier et al., 2003). Internal motion of water drops irradiated by a pulsed

laser was studied (Zardecki and Pendleton, 1989) the results of which showed nearly uniform heating with a small area of intense heating on the rear side for small (10 μm) drops and front surface heating for larger (100 μm) drops.

The laser-induced spark behind a liquid drop, also observed in the present study had been reported much earlier (Astrakhan, 1960). The subsequent breakdown of air under the action of this spark was also studied (Zhuzhukalo et al., 1981). The same process was again studied (Phuoc, 2005) when this laser-induced spark had found ignition applications in internal combustion engines (Phuoc, 2006) due to the several advantages it offers over the conventional spark plug.

In view of the above literature it can be inferred that there is lack of work on the manipulation of liquid drops directly on a solid substrate using pulsed lasers. Expensive and elaborate techniques have been used for the preparation of the hydrophobic substrate. The effect of drop transparency on drop kinematics and laser beam propagation through the drops has also not been demonstrated before. Also, there doesn't exist a theoretical model explaining the physical phenomenon behind laser-induced drop motion, which can work for drops of varying transparency.

1.3 Specific Objectives

In view of the current status concerning droplet-based fluidics, the objectives of the present study are as follows:

1. Production of a simple, inexpensive and disposable hydrophobic substrate and perform measurements of contact angles for different fluids on this substrate.

2. Achieve fluid transport by motion of droplets over the hydrophobic substrate by thermal Marangoni effects through the use of pulsed Nd:YAG laser beam.
3. Develop a photographic technique that works well for visualization of droplets under laser illumination. Use this technique to measure drop kinematics ie. distance traveled, direction of motion , velocity and acceleration at the start of motion.
4. Examine the effect of drop transparency on the drop kinematics.
5. Develop a phenomenological model of the pulsed laser-induced drop motion and validate the model by comparing it to the present experimental results.

1.5 Organization of Thesis

The thesis is organized into four chapters. The first chapter dealt with the introduction, the problem statement, previous studies in this field of study and the specific objectives of this thesis. The second chapter describes the experimental methods. The experimental results and the phenomenological model are discussed in the third chapter. The fourth chapter covers the summary and conclusions and presents avenues for extension of the study. The appendix tabulates the experimental results along with the results of the phenomenological model of this study.

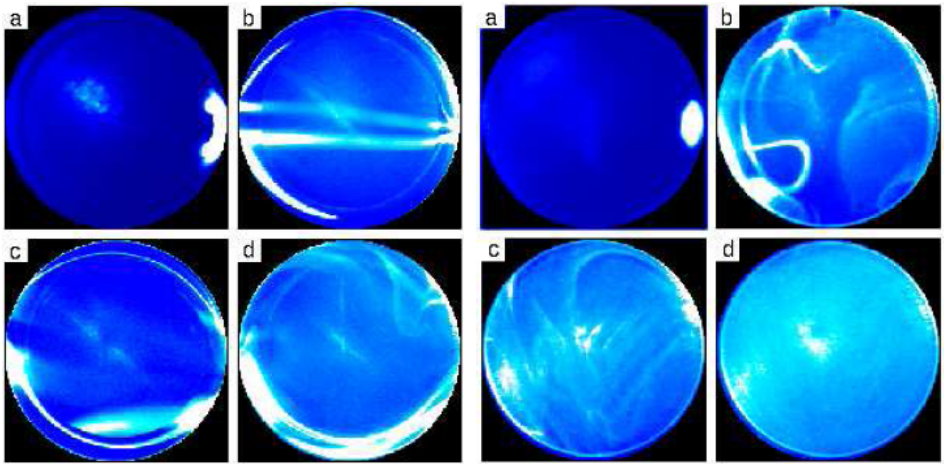

(1) **(2)**

Fig. 1.1. Mixing of fluorescent microspheres in a 3.7 microliter (0.96 mm diameter) undyed droplet by moving the merged drop in one dimension (1) and by motion in two dimension (2). (Grigoriev et al., 2006)

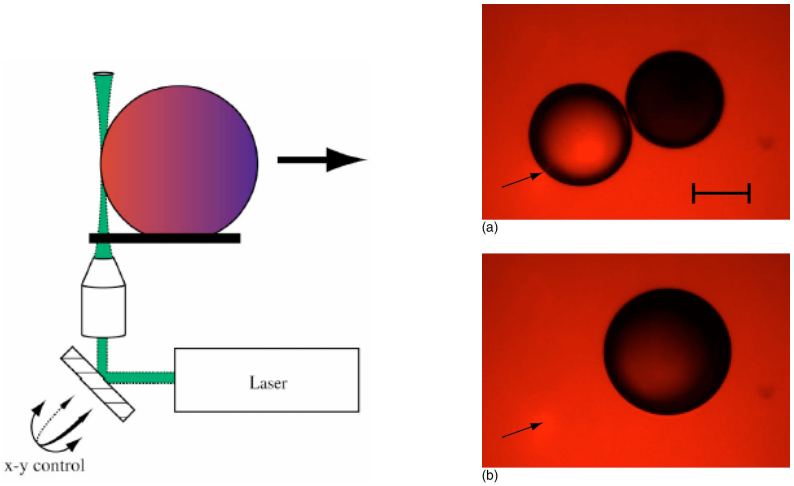

(1) **(2)**

Fig. 1.2. Schematic diagram of the experimental apparatus (1) and the results on mixing of two drops (2). The two frames in (2) are taken at 30 fps, bar represents 100 µm and applies to both panels. (Kotz et al., 2004)

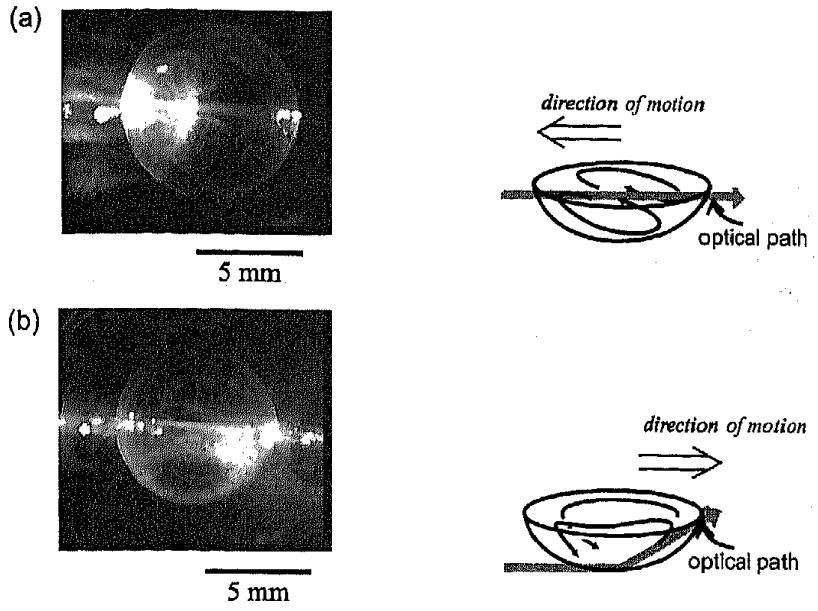

Fig. 1.3. The laser is focused at the oil-air interface (a) and at the bottom of the oil droplet (b). The direction of the laser and the resulting motion is shown alongside. (Rybalko et al., 2004)

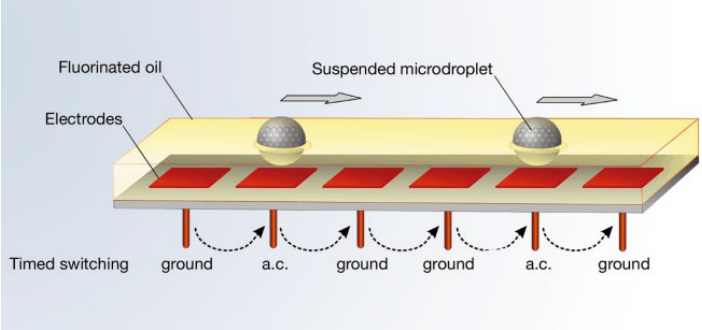

Fig. 1.4. Schematics of the dielectrophoretic transporter used for the operation of a liquid–liquid microfluidic chip with freely suspended droplets. Water droplets in fluorinated oil. (Velev et al., 2003)

CHAPTER II

EXPERIMENTAL METHODS

2.1 Apparatus

The drops required for the present study are produced with a 26-gauge (inner diameter 0.25mm, outer diameter 0.46 mm) syringe needle by mechanically vibrating it. Drops ranging in diameters from 1mm to 4mm were produced this way and analyzed. A hydrophobic substrate on which the drops moved was produced by the application of Fluoropel® PFC M1604V manufactured by Cytonix on a standard glass slide. A thin layer of this liquid which consists of nano-particles in suspension is applied on a regular glass slide and the same is to be heated at a temperature of 70-90^{o}C for about 5 minutes - this was done by keeping it on a halogen lamp, after which the temperature is to be increased to about 175-200^{o}C for further heating for about 15 minutes – this is done on the same halogen lamp with closer contact with the halogen bulb. This results in a solid hydrophobic coating with good glass-adhering properties, good thermal resistance (which is required to resist laser radiation) and stationary water contact angles of up to 170^{o} as shown in Fig. 2.1 (b) and(c). The lasers used in the present study for moving the drops are Spectra Physics model – Quanta Ray: Lab –150, Nd: YAG pulsed lasers. Wavelength is 532nm, pulse frequency is 10 Hz, beam diameter is 9mm and the maximum attainable energy is 300mJ/pulse. The beam diameter is reduced from the initial diameter of 9mm to

a final diameter of 0.9mm using 2 plano-convex lenses with focal lengths of 150mm and 15mm as shown in Fig. 2.2. This intense laser beam is aligned horizontally with the substrate (modified glass slide), on which the drops are present. The laser beam is aligned with the substrate plane by measuring its vertical height (110mm) just after it leaves the laser source and trying to match it throughout its path. By manipulating the position of the laser, which can be done as shown in Fig. 2.2 by reflecting the laser of a mirror and titling the mirror or by moving the substrate on which the droplets are present, the drops can be moved. An energy meter (Ophir Nova II) is placed at the end of the optical path, which records the beam energy. This energy meter comes with a pyroelectric detector with four measuring ranges of 8mJ, 80 mJ, 800 mJ and 8J. For the current experiments 80 mJ energy range is selected. Energies in the range of 3mJ to 12mJ are being used. Energies lower than 3mJ were unable to move the drops whereas at energies higher than 12mJ most drops shattered instead of being propelled. The energy meter can measure both energy and power. Laser energy can be measured with ±0.5mJ error (16%).

A camera (Panasonic DV), which observes the top view of the slide, records the process of drop motion when irradiated by this laser beam. Another camera (Nikon D70) is used to take pictures of the drop along the substrate to measure the contact angles. Images shown in Fig. 2.2 are taken with the Nikon D70.

2.2 Instrumentation

Primarily 3 cameras are used in the present study. The Nikon D70 is used to take a side profile of the droplet to measure the contact angle of the drops. This CCD device has 6.01 megapixels. Lens used on the camera is Nikkor 105mm, f/2.8 D (Micro-Nikkor).

This gives a magnification 240 pixels/mm and a resolution of 60μm as found by the 1951 USAF resolution target, a picture of which is shown in Fig. 2.3. Contact angle from the Nikon images can be read with an error of ±5 degrees (3%). For still higher magnification the Nikon Bellows focusing attachment, PB-6 can be used with the Nikkor 50mm, f/1.4D in reverse. This however comes at the price of loss of depth of view, which gets reduced from 5mm to 2mm. Panasonic DV camcorder is used for imaging the motion of the drops, frame rate is 15 fps, image size is 320*240 pixels and resolution which was determined by observing 3 bar patterns in a picture of a 1951 USAF resolution target taken by this camera as shown in Fig. 2.4, was found to be 180 μm at high levels of magnification. Windows® movie maker is used to convert the video captured into individual frames. Measurements of distance on the DV frames can be made with an accuracy of ±1 pixels (15%). Angle on the frame can be measured with an accuracy of ±2 degrees (80%).

The high speed camera used in the study is IDT model XS-4 (512*512 pixels at 5000 fps maximum and inbuilt memory with storage capacity of 8000 frames). A resolution picture of this camera is shown in Fig. 2.5. The resolution was found to be 60 μm with the Nikkor 105mm lens.

A graph paper is placed below the substrate which serves the dual purpose of aligning the laser and act as a scale for the images. The centerline of the graph paper is aligned with the laser such that the angle of the laser is zero degrees. The laser beam is initially aligned parallel to the x-direction which is the direction of the laser with the help of the graph paper as shown in Fig. 2.6 (a) and (b). The camcorder used to record drop motion was protected from over exposure by a long pass filter (eye protection goggles for

532nm- Glendale 532nm OD5.5), which blocks wavelength of 532nm. This makes the laser completely invisible, making it hard to directly measure the angle the laser beam makes with the x-direction (corresponding to 0^o) at the time of drop motion. The laser beam is moved to different locations using a mirror as shown in Fig. 2.6. This also results in the laser beam not always staying parallel to its initial position. However the exact angle the laser beam makes with the drop motion can be calculated from the location of the drop on the substrate, since the angular displacement of the laser beam from its parallel position can be measured. However, droplets may not always be present at this center position. To measure the angle of the beam with the drop at any given position a picture of the laser beam is taken without the long pass filter which clearly shows the angle of the beam with the x-direction as shown in Fig. 2.6 (c). Direct measurement of the beam angle with the x-direction can be done by removing the filter and taking a picture of the laser beam on the slide. This image can then be used to measure angle correctly using Sigma Scan, however this is not very practical. The angle can also be calculated based on the initial position of the drops on the substrate. The angle was calculated by measuring the distance from the focal plane of the last plano-convex lens to the slide (x) and the distance of the drop above the center of the slide (y). The angle is then found by:

$$\omega = \tan^{-1}(y/x) \tag{2.1}$$

Fig. 2.7 (Hecht, 2001) illustrates this phenomenon with a ray diagram, the rays which are parallel after refraction through the lens appear to come from the focal plane.

The calculated angles found this way agree well with direct measurement. The distance between the plano-convex lens and the center of the slide can be measured with an error of ±1mm (1%). Optics used in the study are 2 aluminized first surface mirrors (Unaxis BD 10307905 VIS) and 2 plano-convex lenses (Thorlab LA4372 and L4917). The individual frames are then analyzed using Sigma Scan® 5.0 which gives the distance moved by the drops and the angle at which the motion occurs. To make measurements easy and accurate the frames are combined to form a single image by 'adding' them together. Since the only moving particle is the drop the image shows a minimal amount of blur. Velocity of the drop is measured by dividing the distance traveled by the drop by the time it took to travel the distance, which is the time interval between consecutive frames (60-70ms) multiplied by the number of frames between the initial and the final position of the drop. The initial acceleration of the drop is measured by calculating the change in the velocity of the drop in the time between consecutive frames.

The surface tension of the test liquids is measured using the Fisher surface tensiometer model 20. Calibration of this device is done in accordance with the procedure given in the instrument's manual. For the measurement of surface tension the standard procedure is applied as given in the manual. A platinum-iridium ring with a circumference of 60 mm is dipped in the solution whose surface tension is desired to be known. The ring is slowly pulled out of the liquid, adjusting the knob on the right side of the case to keep the index lined up with the reference mark on the mirror. The interface on the liquid will become distended, but the index is kept on the reference. These two simultaneous adjustments are continued till the distended film at the interface ruptures.

The scale reading at the breaking point of the film is the apparent surface tension. In order to obtain the true surface tension, the following relationship is used:

$$S = p \times F \tag{2.2}$$

where S is the actual value, p is the apparent value as indicated on the dial reading and F is a correction factor. The correction factor F is dependent on the size of the ring and the size of the wire in the ring, the apparent surface tension and the densities of the two phases (liquid and air). The values of F are obtained from the chart given in the tensiometer manual.

Since the dye acts like a surfactant, the value of surface tension for the dyed solution is much less than that for distilled water.

2.3 Test Conditions

Table 2.1 summarizes the test conditions used in this study. The parameters being recorded are the drop diameter, the drop contact angle, test liquid and the laser beam energy. The liquid used in the study is distilled water with varying concentrations of the fluorescent dye Rhodamine 6G. This dye fluoresces under the current 532nm laser radiation. Amount of dye used for the present experiments varies from 2% of dye by weight to 0.2% of dye by weight. The molecular weight of Rhodamine 6G is 479g, this gives a molar concentration range of 0.041mol/l to 0.0041 mol/l. Concentrations of the R6G have an uncertainty of ±0.1% by weight. By changing the concentration of the dye, drops with varying transparency can be produced and the effect of the transparency on

the angle at which the drop moves, can be studied. The values of surface tension and dynamic viscosity of water for various temperatures are adopted from Incropera and DeWitt (Incropera and DeWitt, 2002) as shown in Table 2.2. The following correlations are used for intermediate values (in SI units). The Seeton fit (Seeton, 2006) is used for viscosity whereas the correlation for surface tension is presented here, the error from both is less than 1% in the range 273.15 to 375 K:

$$\mu_i = 2.414 \times 10^{-5} \times 10^{(247.8/(T_2 - 140))} \tag{2.2}$$

$$\sigma = 6.3173 \cdot T_2^{-0.7865} \tag{2.3}$$

where T_2 is the final absolute temperature (K) of the heated portion of the drop, μ_i is the viscosity of the heated portion of the drop (Ns/m^2) and σ its surface tension (N/m).

The properties of the translucent and opaque solutions at room temperature are tabulated in table 2.3.

Table 2.1. Test Conditions.

Parameter	Range
1. Drop Diameter	1mm – 4mm
2. Contact Angle	150°-170°
3. Test Liquid	[1]Distilled water. [2]Distilled water with varying concentrations of Rhodamine 6G (0.2% - 2% of R6G by weight).
4. Beam Energy	3mJ – 12mJ
5. Non-dimensional number $\sigma\rho d/\mu^2$	15000 - 188000

Table 2.2. Properties of water at various temperatures.

Temperature, K	Dynamic Viscosity, μ_i (10^{-6} Ns/m^2) [a]	Dynamic Viscosity, μ_i (10^{-6} Ns/m^2) Correlation [b]	Surface Tension, σ (10^{-3} N/m) [a]	Surface Tension, σ (10^{-3} N/m) Correlation [b]
273.15	1750	1753	75.5	76.6
275	1652	1653	75.3	76.2
280	1422	1421	74.8	75.1
285	1225	1235	74.3	74.1
290	1080	1083	73.7	73.1
295	959	958	72.7	72.1
300	855	854	71.7	71.2
305	769	767	70.9	70.2
310	695	692	70.0	69.4
315	631	629	69.2	68.5
320	577	575	68.3	67.6
325	528	527	67.5	66.8
330	489	486	66.6	66.0
335	453	450	65.8	65.3
340	420	419	64.9	64.5
345	389	390	64.1	63.8
350	365	365	63.2	63.0
355	343	343	62.3	62.3
360	324	323	61.4	61.7
365	306	305	60.5	61.0
370	289	288	59.5	60.3
373.15	279	279	58.9	59.9
375	274	274	58.6	59.7

[a] From Incropera and Dewitt, (2002).
[b] From correlation, equation 2.2 and 2.3

Table 2.3 Properties of Translucent and Opaque solutions at room temperature.

Solution	Concentration (Dye % by weight)	Surface Tension, σ (10^{-3} N/m)	Density, ρ (kg/m^3)	α, absorbance (% absorptance)
1. Translucent	0.2	50	998	1.1-1.7 (93-96%)
2. Opaque	2	53	1015	2.1-11.9 (97-100%)

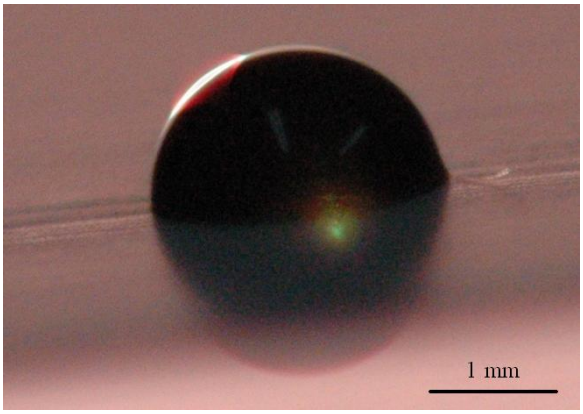

(a)

(b)

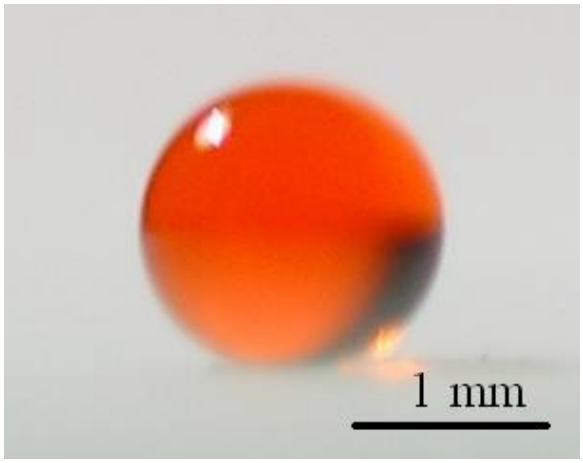

(c)

Fig. 2.1. (a) a colored drop (food dye) on substrate made using Teflon tape, contact angle 85° (drop diameter 2.3mm) (b) a transparent water drop on the Fluoropel® substrate, contact angle 169° (drop diameter 1.7 mm) (c) contact angle for a colored (Rhodamine 6G, 0.2% by weight) drop on Fluoropel®, contact angle 170° (drop diameter 1.6mm).

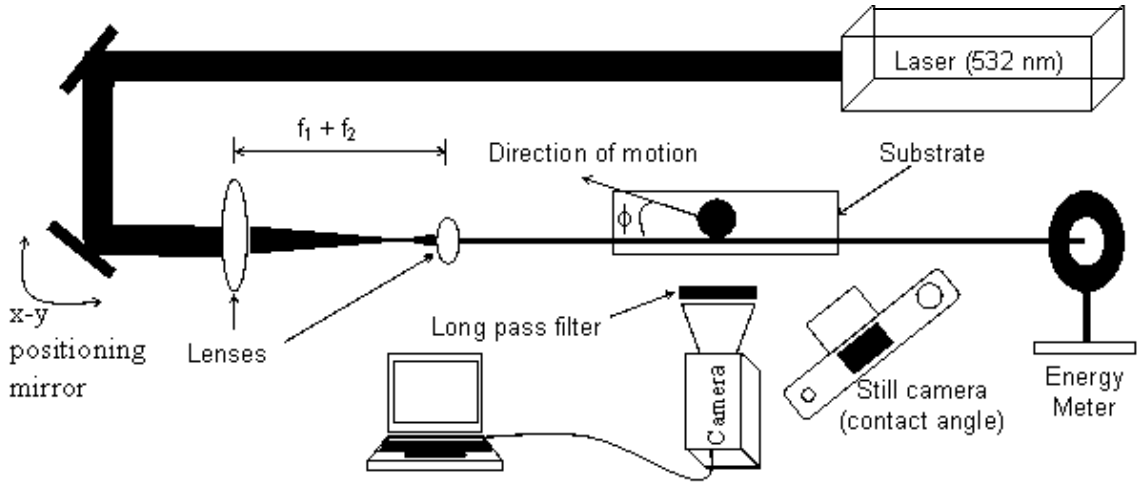

Fig. 2.2. Set up used for study. Camera connected to the computer observes the top view of the substrate.

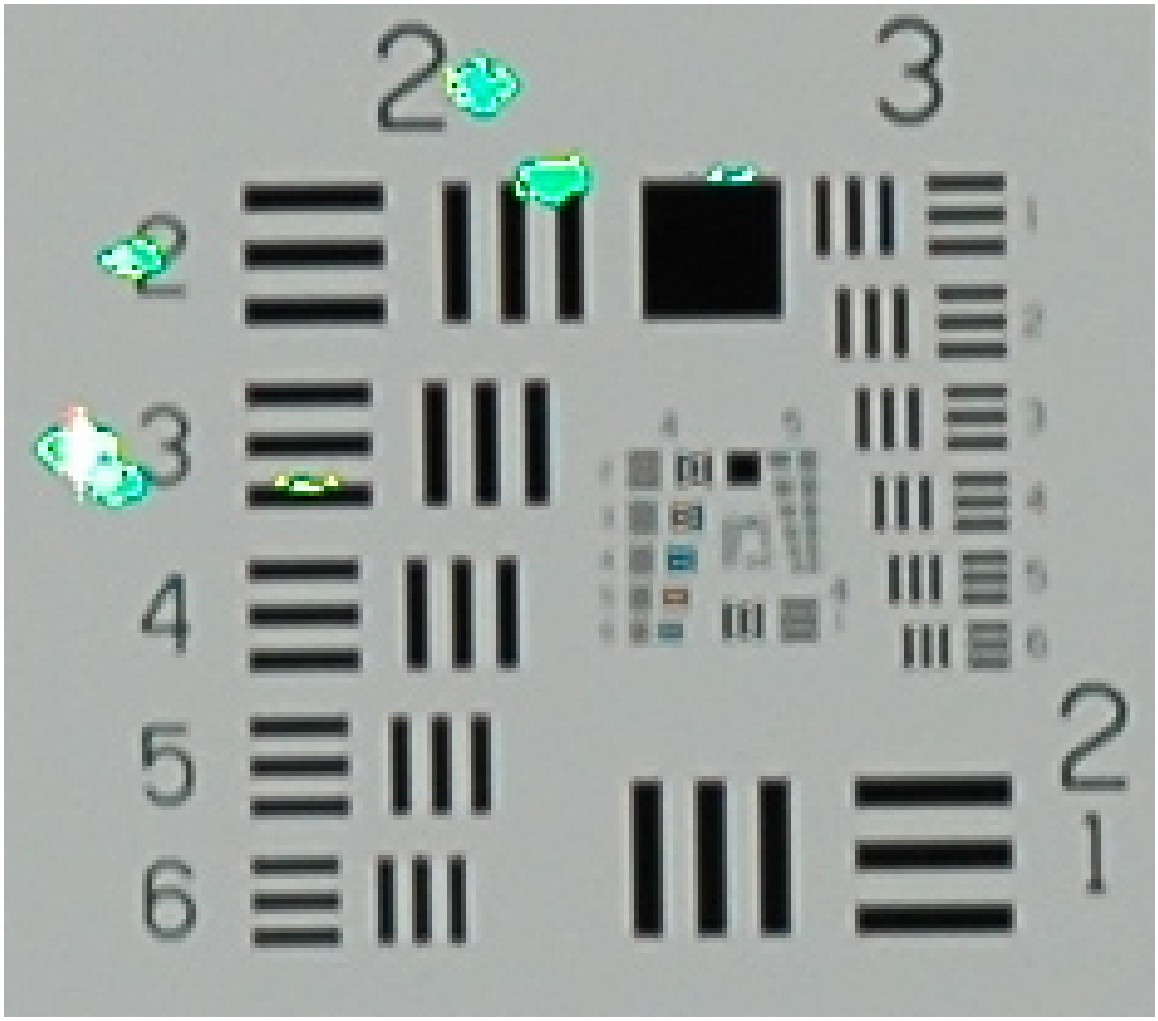

Fig. 2.3. Picture of the 1951 USAF target used to calculate the resolution of the NikonD70, still camera (60μm).

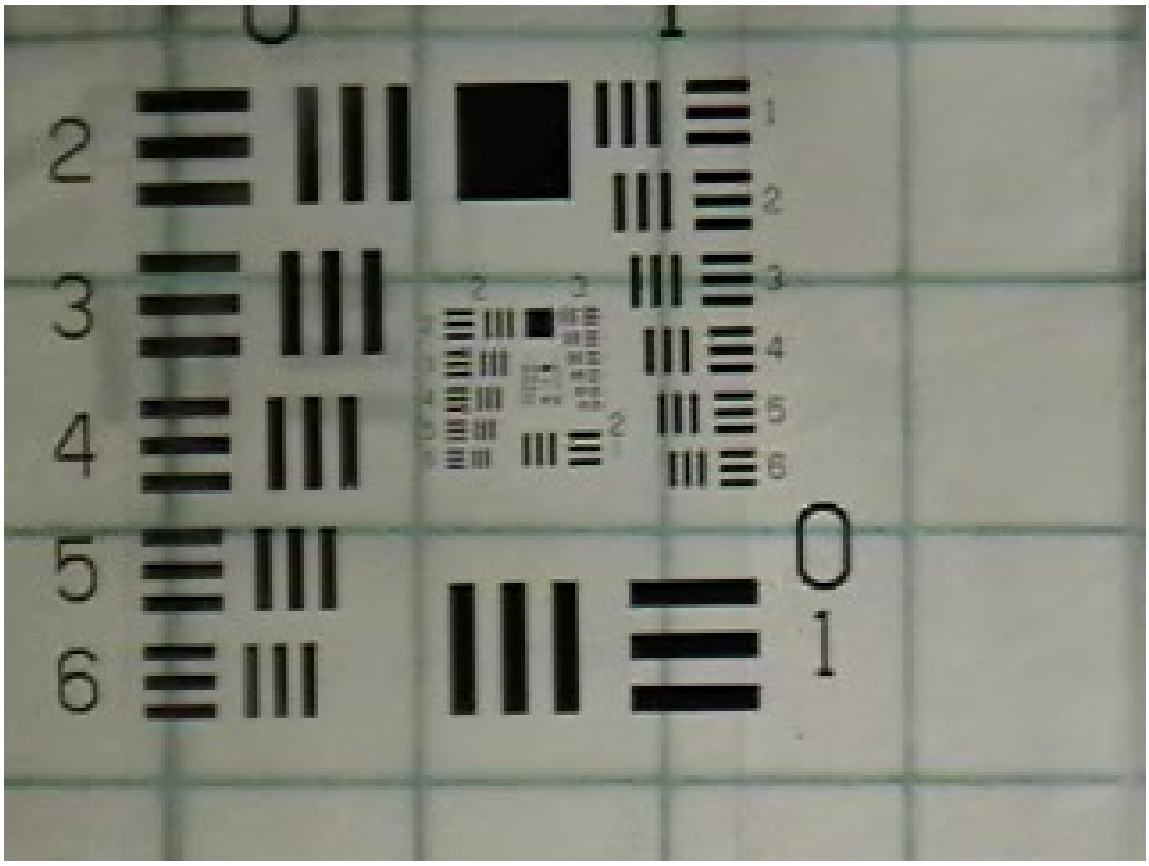

Fig. 2.4. Picture of the 1951 USAF target used to calculate the resolution of the camcorder (180μm).

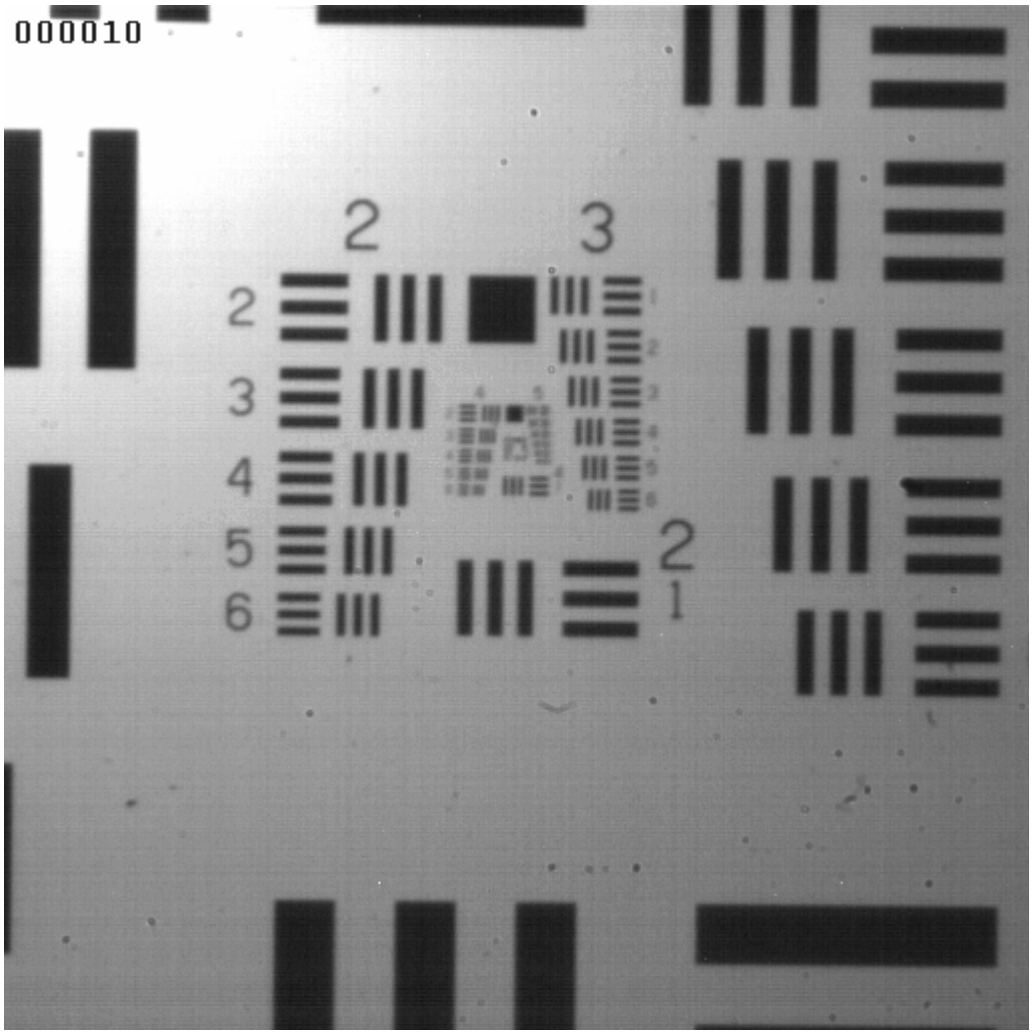

Fig. 2.5. Picture of the 1951 USAF target used to calculate the resolution of the High-speed camera (60μm).

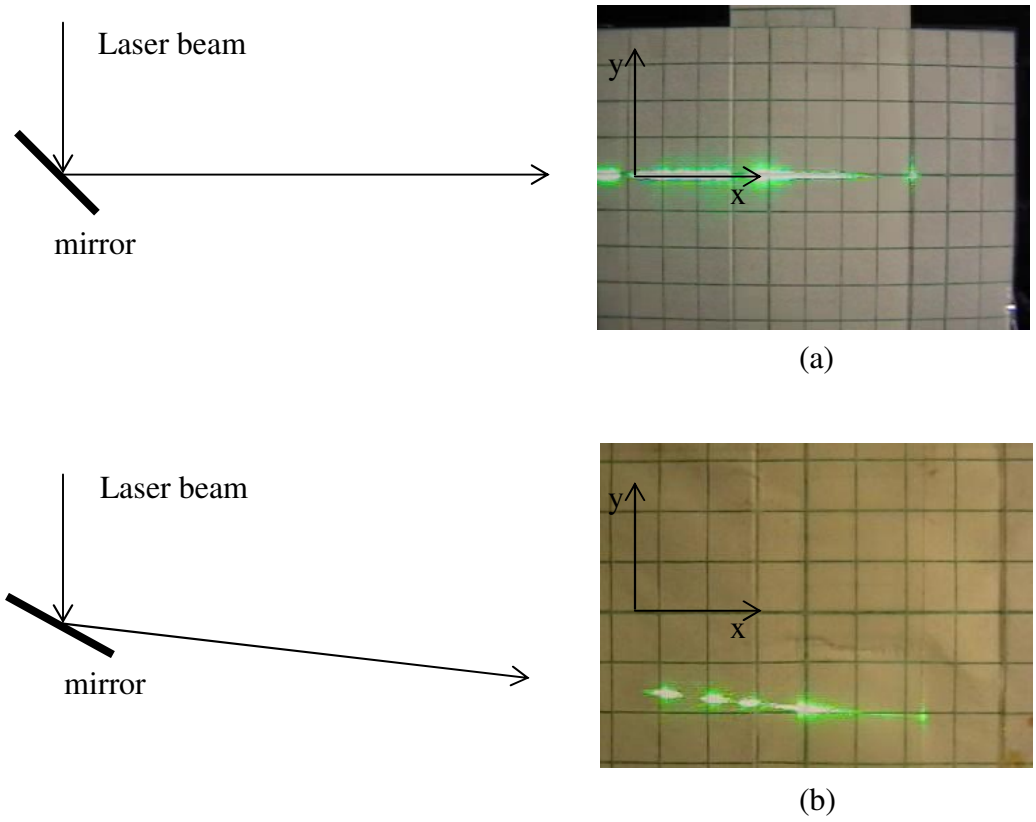

Figure 2.6. (a) shows the beam aligned with x – direction such that it makes an angle of 0 degrees with the x - direction. (b) shows the beam making an angle with the x – direction.

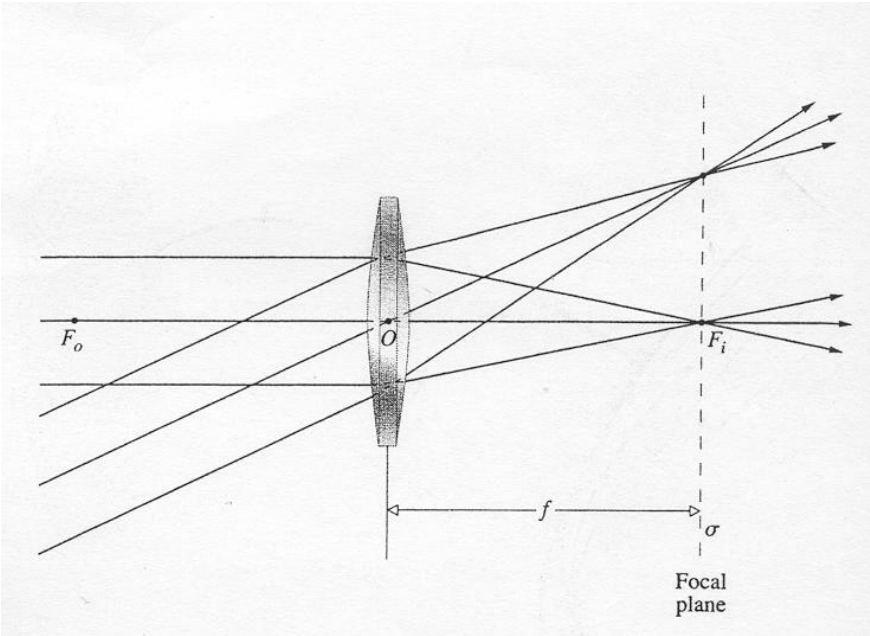

Fig. 2.7. The focal plane of a lens. Used to calculate angle of the beam with the horizontal for various locations of the beam. (Hecht, 2001)

CHAPTER III

RESULTS

3.1 Direction of motion

Drops with contact angles of 160±10 degrees were used in this study. Drop velocities in the range of 11mm/s to 240mm/s are observed, with a mean velocity of 130mm/s. The motion of the drop does not take place normal to the beam, as observed by earlier researchers (Kotz et al., 2004) who used a different set up – where the beam was introduced from the bottom, such that it came through the substrate rather than along it, nor does the drop always move along the beam as one would imagine intuitively. When a drop is heated non-uniformly it develops a surface tension gradient along its surface due to the thermal gradient ie. thermal Marangoni effects. The highest surface tension occurs on the coldest part of the drop and the lowest surface tension develops on the hottest part of the drop. This surface tension gradient induces a net force, the actuating force for motion F_{act}, which pulls the drop in the direction of the cold part of the drop. Unlike previous (Grigoriev et al., 2006) thermal Marangoni migrations, where the drop that is moved is present in suspension form in some other liquid and moves in it, here the drop is heated directly and moves directly on a solid substrate, the heating taking place at a liquid-gas interface. For a transparent drop as the laser passes through the drop, the drop acts like a ball lens with a definite focal length.

The focal length, f is given by:

$$f = \mu d/4(\mu-1) \qquad (3.1)$$

where d is the drop diameter and μ is the refractive index of the water drop. For a water drop diameter of 1mm, f is 1mm and for a water drop of diameter of 4mm, f is 4mm as calculated by the above formula.

As the laser beam converges at the focal point of this liquid ball lens it results in the production of a spark, distinctly visible at high laser beam energy (6mJ) and even producing a loud clicking sound due to the ionization and breakdown of the air at the spark (Zhuzhukalo et al., 1981). This optical breakdown results in the formation of plasma (Autric et al., 1988) that absorbs much of the incident laser radiation. The motion of the drop takes place nearly diametrically opposite to this hot spot or spark for transparent and near transparent drops due to the thermal gradient that the hot spot generates. For a transparent drop this is schematically represented in Fig. 3.1 (a). The first frame shows the spark behind the drop.

Now as the drop is made less transparent and more toward being completely opaque by adding increasing amounts of the dye (Rhodamine 6G) the intensity and thus the heating effect of the spark steadily falls off. This results in larger angles between the drop motion and the beam direction. For a translucent drop some of the laser is transmitted, some of it is reflected back and most of it is absorbed along the drop thus the drop heats up along the laser path as shown in Fig. 3.1 (b). This results in almost perpendicular motion to the laser.

For an opaque drop, negligible percentage of the laser is transmitted through the drop, most of the laser is absorbed by the drop at the first surface and some is lost as emissive radiation resulting in a thermal gradient along the drop as shown in Fig. 3.1 (c). This results in motion at very large angles with the oncoming laser. The bright spot on the last frame is from the fluorescence of a drop.

The angles at which various drops have moved are shown in Fig. 3.2 where 0^o is the beam direction. The radius axis represents the distance moved by each drop, distance (x) being normalized by drop diameter (d). The droplets that move at smaller angles are transparent, while those that move at about 90^o are translucent and the ones that have moved at larger angles still are nearly opaque. The distance moved by each drop follows a lor-normal profile, with most of them moving about 5 drop diameters as shown in Fig. 3.3. The average distance that the drops move is also calculated to be 5 drop diameters.

3.2 Model for drop motion

The power flux incident on the drop (E_i) W/m^2 and the flux absorbed by the drop (E_a) W/m^2 are given as follows:

$$E_i = P/A_l \tag{3.2}$$

$$E_a = aE_iA_l \tag{3.3}$$

where P is the power of the laser in watts (4.6 – 12.0mJ per pulse), A_l is the cross sectional area of the laser beam (diameter 0.9mm) in m^2 and a is the absorptance of the

drop (0.002 – 1), which depends on its transparency. Typical numbers for E_a are between 9.8×10^{-6} W to 4.1×10^{-5} W for transparent drops and 0.06 to 0.12 W for dyed drops. The absorption coefficient of Nd:YAG 532nm laser radiation by pure water, which is used to calculate the absorbance and the absorptance, is $c_a = 0.05\ m^{-1}$ (Pegau et al., 1997) and the absorption coefficient of Rhodamine 6G solution is $c_a = 150\ m^{-1}$ for a concentration of 2.14×10^{-5} mol/l and $c_a = 600\ m^{-1}$ for a concentration of 8.55×10^{-5} mol/l as measured by (Bindhu et al., 1999). The absorption coefficient for Rhodamine 6G is approximated to have a nearly linear dependence on concentration for 532nm as shown by them (Bindhu et al., 1999). The absorbance and absorptance calculated from the absorption coefficient this way is required to find what fraction of the incident radiation is absorbed by the drop and in the case of near total absorbance, what is the length that the laser travels within the drop. Unlike solids, the absorbed flux depends not only on the surface and the incident flux, but also on the distance the radiation traverses in the medium, called pathlength (L). Based on the given values of the absorption coefficient ($c_a\ m^{-1}$) (Bindhu et al., 1999), the values of absorbance (α) and absorptance (a) are calculated as follows:

$$\alpha = c_a l \tag{3.4}$$

$$a = 1 - 10^{-\alpha} \tag{3.5}$$

where absorptance (a) is the ratio of the absorbed flux (E_a) to the incident flux (E_i).

$$a = E_a/E_i \tag{3.6}$$

The maximum value of (a) can thus be equal to one, in which case all of the incident flux is absorbed by the drop.

Radiation losses dominate at the start of the motion since time interval is small for convection and conduction losses to occur, however it is convection and conduction heat transfer that eventually reduce the thermal gradient below a certain limit. This makes the actuating force (F_{act}) fall below the limit needed to push the drop forward. The radiation loss (E_e) from the drop is given by:

$$E_e = \varepsilon(5.76E\text{-}8)A_h(T_2^4 - T_1^4) \tag{3.7}$$

where ε is emissivity of the drop liquid which is the same as its absorptivity based on Kirchoff's law, 5.76E-8 W/m^2K^4 is the Stefan-Boltzman Constant, A_h is the heated area of the drop which is calculated from geometry as shown in Fig. 3.4 as follows:

$$A_h = 2\pi HR \tag{3.8}$$

where H and R are as shown in the Fig. 3.4, T_2 is the final absolute temperature of the drop and T_1 the ambient temperature in K. Calculations show E_e to be between 8.8×10^{-8} W to 1.4×10^{-7} W for transparent drops, 4×10^{-4} W to 5×10^{-5} W for translucent drops and 5×10^{-4} W to 4×10^{-2} W for opaque drops. The rise in temperature of the heated portion of the drop can be calculated from the following heat balance:

$$E_a - E_e = mcdT/dt \quad (3.9)$$

where m is the mass of heated region in kg, which is the mass of the spherical cap and depends on transparency as will be explained in section 3.4 and c is the specific heat capacity of water (4200 J/kgK). E_a and E_e are the energies absorbed by the drop and emitted by the drop respectively and are found from calculations. It is this rise in temperature (dT) that induces the surface tension imbalances ($\Delta\sigma$), which in turn produce the force required for the motion. For calculation of dT, the time interval dt is taken to be 0.8 s for transparent drops and 0.5 s for dyed drops. This corresponds to 8 and 5 laser pulses respectively. This is approximated from the video for the motion and also based on observations such as the numbers of clicks heard from the spark before motion is initiated. The final temperatures reached by the heated portion of the drops based on direct laser heating are calculated to be between 315 K and 580 K. These high temperatures can also explain why some drops explode when irradiated by pulsed laser instead of being propelled. Temperatures as high as 2400 K have been reported by other researchers (Carls and Brock, 1987) who studied droplet explosion by pulsed lasers. This rise in temperature is small for transparent drops because most of their heating comes from the spark and not directly from the laser, and large for opaque drops which receive most of their heating directly from the laser. The rise in temperature was estimated from calculations assuming convection and conduction heat transfer within the drop to be negligible during the short time interval dt, further experimental studies can be undertaken to verify the accuracy of such calculations such as actual temperature measurement by use of an infra-red camera.

3.3 Force Balance

The angular direction of this motion depends on how the drop is heated, which is determined by its absorbance. The surface tension gradient which develops on the drop can be approximated as shown in Fig. 3.5. The cooler side has a higher surface tension (σ_c) and the heated side had a lower surface tension (σ_h), thus there is a force (F_{act}) in the direction of the cooler region which pulls the drop toward the cooler region. The actuating force (F_{act}) being a surface force, depends only on the surface tension gradient ($\Delta\sigma$) and the effective circumference between the cooler and the heated sides of the drop. The actuating force (F_{act}) due to surface tension difference along the drop is given by the following expression:

$$F_{act} = 2\pi r(\sigma_c - \sigma_h) \tag{3.10}$$

where r is the radius (m) of the heated region (the spherical cap) which is calculated from geometry as explained later (Eq. 3.24 and 3.30), σ_c and σ_h are the surface tension at the ambient temperature (T_1) and the heated temperature (T_2) in N/m respectively. Values of F_{act} range between 1.5×10^{-5} N to 7.6×10^{-5} N. Even though Radiation pressure (F_{RP}) or the photoreactive force (Ivanov et al., 1977) given by:

$$F_{RP} = P/\upsilon \tag{3.11}$$

also adds to F_{act}, where P is the laser power in watts and υ is the speed of light in m/s but calculations show that this force (2.6×10^{-10} N to 3.3×10^{-10} N) is much less than the F_{act} calculated in Eq. 3.10. The resisting force (F_{res}) of the motion comes from the aerodynamic drag (F_{aero}) and the surface resistive drag (F_{sres}), which is the surface drag for a drop traveling on a solid substrate as follows:

$$F_{res} = F_{aero} + F_{sres} \tag{3.12}$$

The aerodynamic drag is given by:

$$F_{aero} = 6\pi r\mu_0 u(1+2\mu_0/3\mu_i)/(1+\mu_0/\mu_i) \tag{3.13}$$

where r is the radius of the drop, μ_0 is the dynamic viscosity of air and μ_i is the dynamic viscosity of water. The above expression is for creeping flow past a fluid sphere (White, 1991). An empirical constant based on flow characteristics needs to be added to the above expression to accommodate for the present higher Reynolds numbers and the wall effect (Ataide et al., 1999; (Chen, 1999; (Chen, 2000). Values of F_{aero} range from 6.2×10^{-9} N to 1.6×10^{-7} N. The surface resistive force dominated by surface drag (Yang et al., 2004) is given by:

$$F_{sres} = \sigma_c f_1 w(\cos\theta_R - \cos\theta_A) \tag{3.14}$$

where f_l is the length fraction of drop that actually makes contact with the substrate (Yang et al., 2004), w is the contact diameter (m), θ_R is the receding contact angle and θ_A is the advancing contact angle. These angles are found to be 5 degrees ± from the stationary contact angle measured. Typical values of F_{sres} range in between 6.5×10^{-8} N to 2.0×10^{-7} N.

Applying a force balance the following result can be obtained, as shown in Fig. 3.6:

$$F_{Net} = F_{act} - F_{aero} - F_{sres} \tag{3.15}$$

from this equation the acceleration of the drop can be found. However, this is the acceleration at the start of the motion, with the progress of time F_{act} decreases as ΔT decreases steadily, so does $\Delta\sigma$. So F_{act} is not steady and also, the aerodynamic drag F_{aero} depends on the velocity of the drop and therefore is not constant throughout the motion. To find the acceleration at the start of the motion F_{aero} and F_{sres} are set to zero. Fig. 3.7 shows the acceleration based on their drop diameters and transparency. Acceleration is found to increase as the drop diameter reduces. Also, opaque drops accelerate faster than transparent drops.

3.4 Energy Balance

The net force (F_{net}) acting on the drop is not a constant force and hence the drop does not have any constant acceleration, but only a time dependent acceleration. Therefore to find the distance traveled by the drop, an energy balance is required. Unlike

force, all the energy gained by the drop is gained at the start of the motion, the drop does not gain any energy once it is no longer in contact with the laser beam. This energy is then dissipated in doing work against the resisting force, which gives the total distance traveled by the drop. Rise in temperature ΔT, causes a rise in volume of the heated region of the drop Δv and consequently a rise in the surface area of the heated region ΔA_h, which results in the rise of the surface energy, SE. This SE is then converted into the kinetic energy (KE) of the drop to produce motion. The drop is heated as shown in Fig. 3.4. By simple geometric relations, the volume of the heated region (the spherical cap) is given as follows:

$$v = \pi H^2(R-H/3) \tag{3.16}$$

Where v is the volume of the heated region (m^3), H is the diameter of the laser and R the radius of the drop. Due to a temperature rise in the drop, the heated volume of the drop expands by Δv which can be found by knowing the coefficient of thermal expansion for water (β = 0.3E-3 /K) and assuming the change in volume changes the radius (ΔR) only and does not effect H of the heated region. Typical numbers for Δv are 10^{-11} m^3 or 10pl (1-28% increase). This Δv increases the surface area by an amount given by ΔA_h as follows:

$$\Delta A_h = 2\pi H(\Delta R) \tag{3.17}$$

This change in surface area increases the surface energy of the drop (SE), which is given by the following relation:

$$SE = \sigma_c \Delta A_h \tag{3.18}$$

This rise in surface energy (SE) is converted into the kinetic energy of the drop where it is dissipated in doing work against the resisting force by traveling a distance s as follows:

$$s = SE/ F_{res} \tag{3.19}$$

It is observed that the drop slides on the substrate. Thus there is shearing at the drop and substrate interface. Typical numbers for s calculated from the model are around 120mm which closely follow experiments. Comparative results of the observed experimental data and the model for distance traveled are given in Fig. 3.8.

To apply the model to the drop, the heated region of the drop which is exposed to the laser is divided into 10 cells as shown in Fig. 3.4, with varying volume and surface area so they contribute to the F_{act} in proportion to their areas, this is what determines the angle at which the drop will move. As explained earlier, the absorbed flux for a liquid depends on the absorptance (a, whose maximum value can be 1) and the pathlength (L). If however on calculating as shown in equations 3.4 – 3.6, the value of (a) comes out to be very close to 1 then the depth of penetration for 90% absorption is calculated. This implies that the pathlength (L) chosen initially to be equal to 2x as shown in Fig. 3.4, is not the actual path length in this case, since almost all the incident flux is absorbed before

the laser can traverse the entire depth of the drop. So a new pathlength is calculated for 90% absorption, based on this pathlength, the number of cells of the drop that will be heated can be calculated. The following inference can be incurred from this, if $L > 2x$, then the laser exits the drop and if $L \leq 2x$, then the laser doesn't exit the drop, and so the energy transmitted through the drop $E_t = 0$. In the latter case the pathlength required for the near total absorption of the laser or length for which $a = 0.9$ is found as explained. Based on the number of cells penetrated the angle at which the drop moves can be calculated as shown in Fig. 3.4. Subsequently the heat balance, the force balance and the energy balance are applied to these n cells. The various parameters of the drop (y_n, z, x and L) are calculated based on the drop geometry as follows, Fig. 3.4 shows the various parameters of the drop geometry being calculated.

$$x = (r^2 - (r-H)^2)^{0.5} \tag{3.20}$$

$$lp = ((r-H)^2 + ((5-n)x/5)^2)^{0.5} \tag{3.21}$$

$$\delta = \sin^{-1}((r-H)/lp) \tag{3.22}$$

Applying the sine rule to the triangle:

$$(lp/\sin\psi) = (r/\sin(90+\delta)) = (y_n/\sin\gamma) \tag{3.23}$$

from the above equation the value of y_n (n = 1 to 10) can be found. The heat balance is applied to the volume of the spherical cap formed by these n cells that the laser penetrates.

The value of z is found depending on the value of n also as follows:

$$z = ((y_n)^2 + (nx/5)^2)^{0.5} \tag{3.24}$$

motion of the drop is then assumed to occur normal to z. The angle with the beam, φ (in degrees) as predicted by the model is thus given by:

$$\varphi = (\tan^{-1}(y_n /(nx/5)) + 90) \tag{3.25}$$

The above description was for opaque and nearly opaque drops, basically drops in which most of the heating comes directly from the laser irradiation. In the foregoing discussion refraction and reflection effects within the drops were ignored due to the small size of the drops. However, multiple reflections and refractions are possible within the drops coupled with light scattering from the fluorescent dye. Inclusion of such effects may make the model more accurate. For a transparent drop, the above procedure needs to be repeated, appended by the following analysis.

Almost all the energy exiting the drop (E_t) goes into formation of the spark. This was observed during experiment, where the energy meter showed very small reading whenever there was a spark. Heat emitted form the spark is what heats a transparent drop.

Assuming the spark emits like a black body (Phuoc, 2005), its temperature can be found as follows:

$$E_t = (5.76E\text{-}8)A_s T_s^4 \tag{3.26}$$

where A_s is the area of the spark, from picture (observed) and T_s is the absolute temperature of the spark. A temperature in the range of $10^5 – 10^6$ K was calculated for T_s, which is in good agreement with observations of other researchers (Phuoc, 2005), where various methods have been implemented to find the temperature. Interestingly the heat emitted from the spark is not emitted uniformly in all directions, most of the heat emitted is emitted in the direction of the oncoming laser (Beduneaua and Ikeda, 2004). There is creation of plasma and a shock wave is created traveling away from the spark toward the laser (Zakharin et al., 1999). This can also explain the loud clicking sound observed during the creation of a spark. The high temperature shock wave and plasma, which carries most of the spark energy, is what pushes the drop. It would be hard for the drop to heat itself from the spark only through radiation, since its absorbance is still the same (very low).

So flux absorbed by the drop from the spark, E_{spark} is:

$$E_{spark} = E_t - E_{losses} \tag{3.27}$$

E_{losses} are estimated to be about 40% of the flux that comes into the spark (E_t). So the net flux deposited in a transparent or near transparent drop (in which the laser exits and forms a spark) is:

$$E_a - E_e + E_{spark} = mcdT/dt \tag{3.28}$$

After the calculation of dT/dt, the same procedure as for an opaque drop for force and energy balance needs to be applied.

The actuating force is then calculated based on only the dimensions of the heated region of the drop.

$$F_{act} = 2\pi r(\Delta\sigma) \tag{3.29}$$

where r is the radius of the heated region and $\Delta\sigma$ is the change in surface tension, N/m. The value of r is given by:

$$r = ½\ z \tag{3.30}$$

where z is as calculated above (Eq. 3.24). The drop moves normal to the plane of z, thus giving the required angle of drop motion, ϕ. The more opaque the drops is the lesser are the cells that the laser beam will penetrate, thus the angle at which it moves will be greater as can be seen in Fig. 3.4. The numbered arrows (3, 6 and 7) in Fig. 3.24 show the direction of motion corresponding to the number of cells the laser beam penetrates (3, 6

and 7) within the drop. For a transparent drop since heating comes from the spark the drop will move toward the laser, resulting in the lower angles observed.

3.5 Model Validation

The prediction of the model and the experimental results of the angular displacement are shown in Fig. 3.9. The angle found for transparent drops from the code is not unique, since they are processes that the model does not account for like plasma formation around the spark and the shock wave emanating from the spark, for every individual drop, which is reflected in the wide variation between calculated and observed angles for transparent drops. The agreement between the two values is more at higher concentrations of R6G where the model calculates a unique angle for every individual drop based upon the input parameters. The ratio of the distance traveled by the drop to that predicted by the model is shown in Fig. 3.10. The model works well for Re higher than 10. At lower Re it under predicts the distance moved by the drops. It is also found that the ratio of the distances as observed and as predicted by the model stack up at around the 25000 value of the non-dimensional number $\sigma\rho d/\mu^2$, showing that the present tests are being performed at that value of the non-dimensional number.

Variations between the model and the experiments exist because the model is simplified, there are processes taking place that the model does not account for (the shattering and vaporization of drops, and the properties of the spark induced, creation of plasma around the spark, the shock wave formation from the spark). The model deals with the special case of the laser beam always being at the side of the drop, However this special case that the model deals with is a very “general” special case because doesn’t

matter at which point the laser was when the drop actually moved, the laser was at the position the model assumes at some point and since the laser is made to scan on the substrate very slowly it is safe to assume that the most of the heating took place in the position assumed in the model.

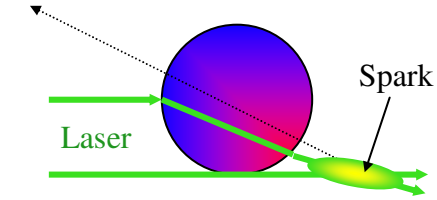

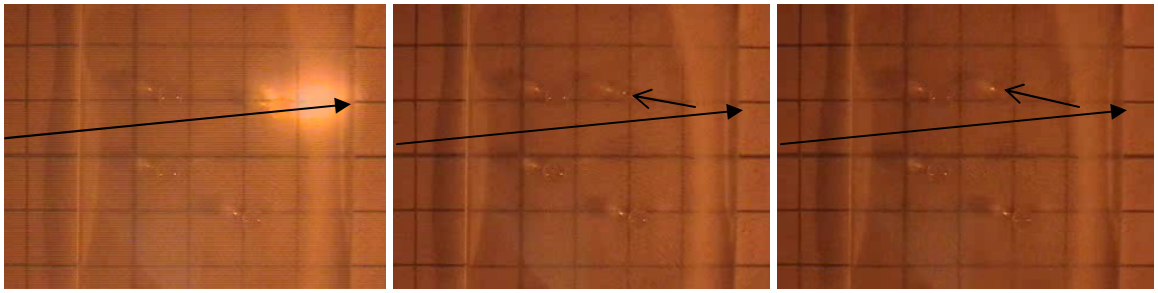

(a) Transparent drop

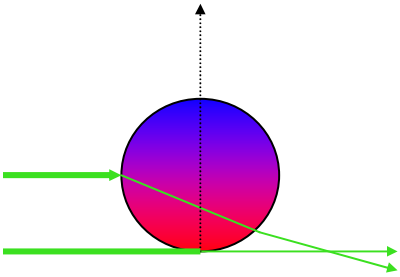

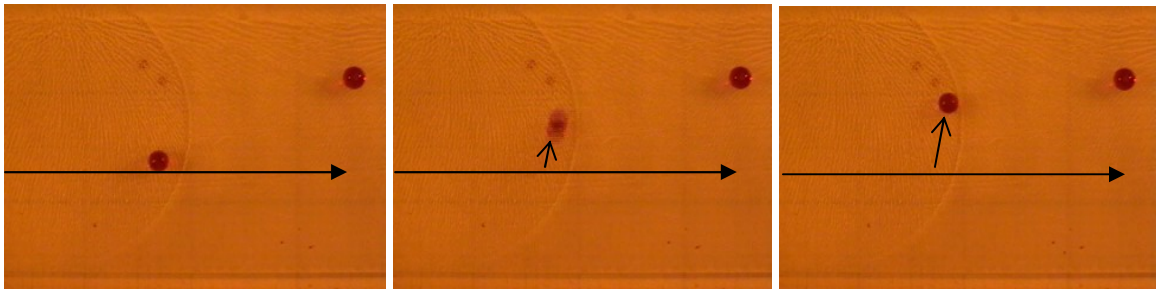

(b) Translucent drop

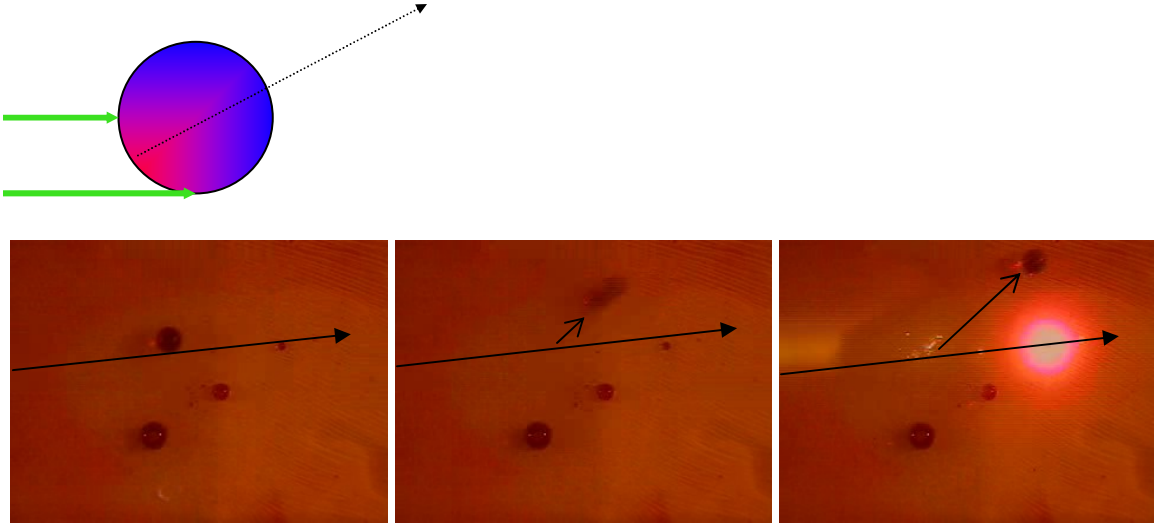

(c) Opaque drop

Fig. 3.1. Schematic of the motion of drops (shown by dotted arrow). Red represents hot regions and blue represents cold regions. Thermal gradient on various drops and 3 frames from the subsequent motion as observed, square edge is 5.08 mm in (a) and 10 mm in (b). Long arrow on the frame represents laser beam direction, small arrow shows the direction of motion.

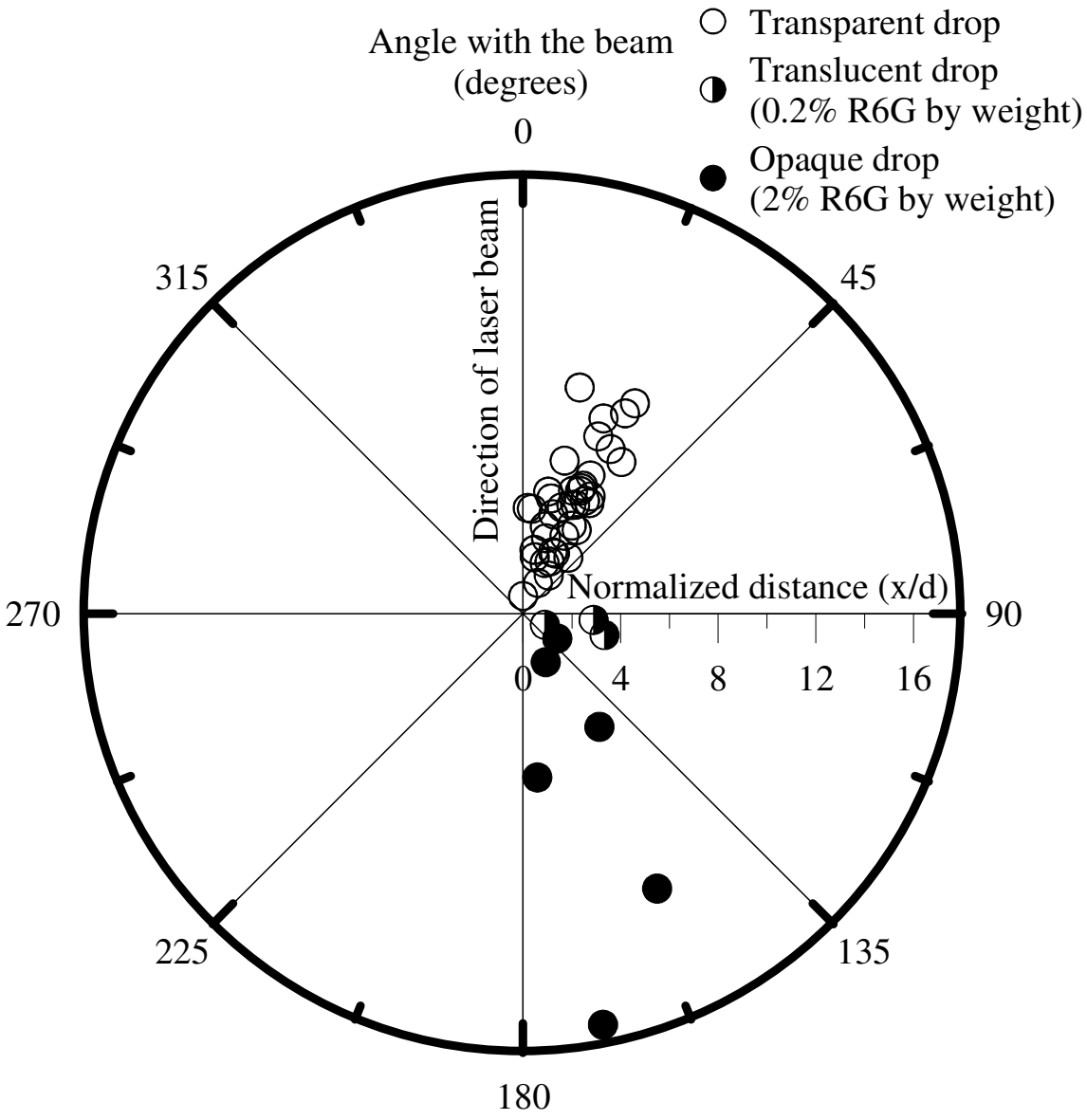

Fig. 3.2. Distribution of motion of various drops. 0^o represents the beam direction.

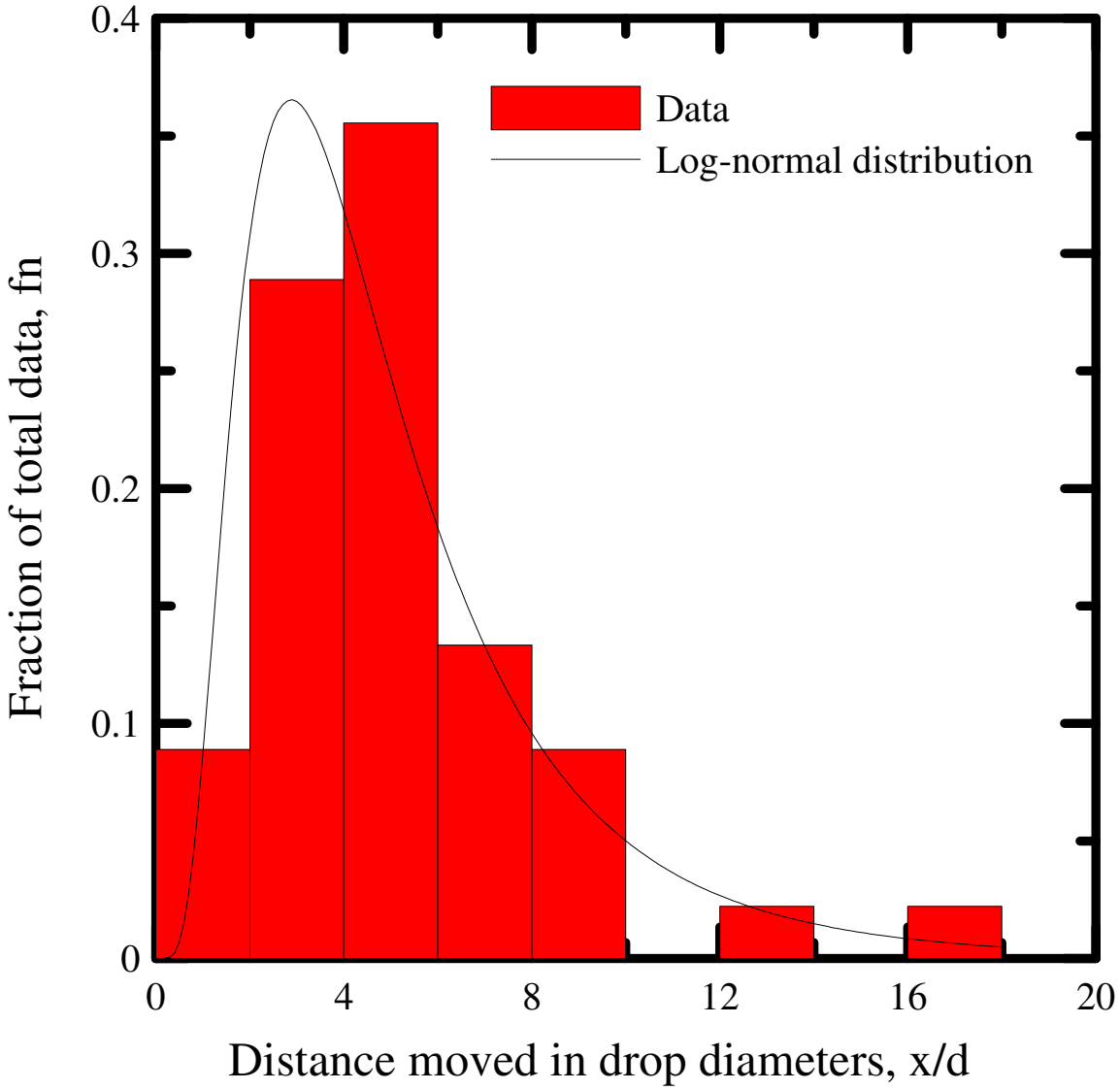

Fig. 3.3. Distance moved by the drops in drop diameters. Distance moved follows a log-normal profile.

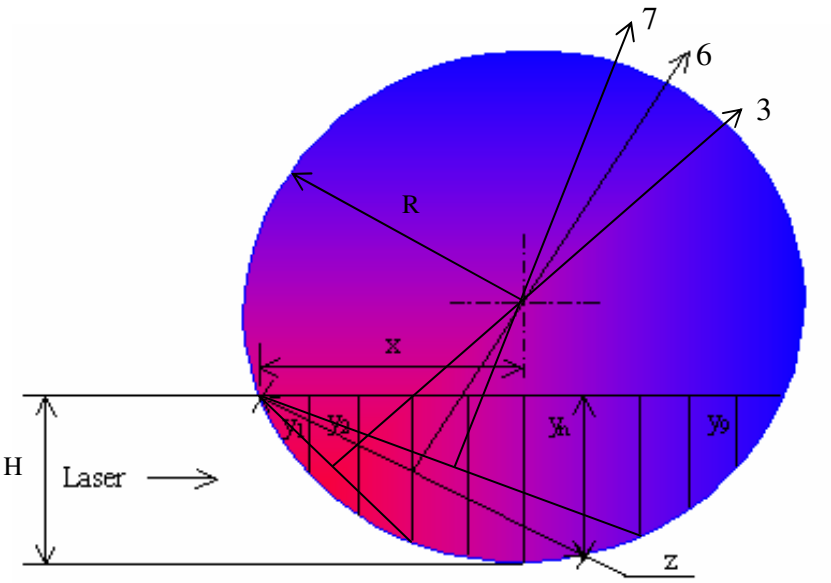

Fig. 3.4. Schematic of the geometry used to calculate the heated volume and area. The heated volume is divided into 10 cells for the model.

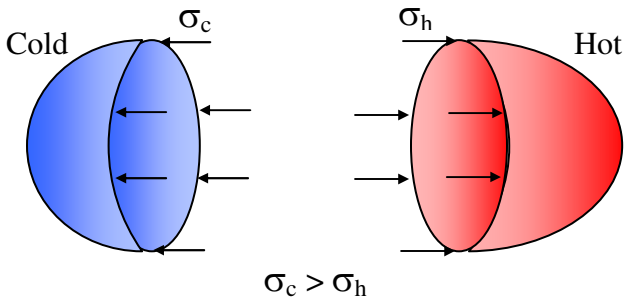

Fig. 3.5. Schematic representation of the surface tension imbalances. The volume and the area of the heated region is more than the cooler region, resulting in the surface energy (SE) rise, which is converted to the drop kinetic energy (KE).

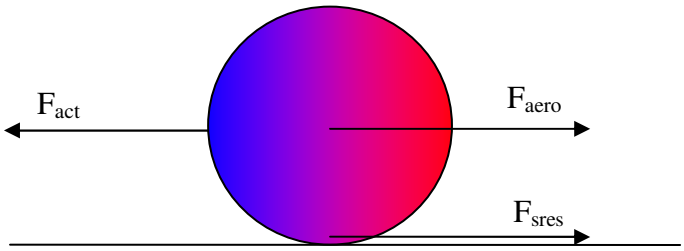

Fig. 3.6. Force balance on the drop. Red is hot, blue is cold.

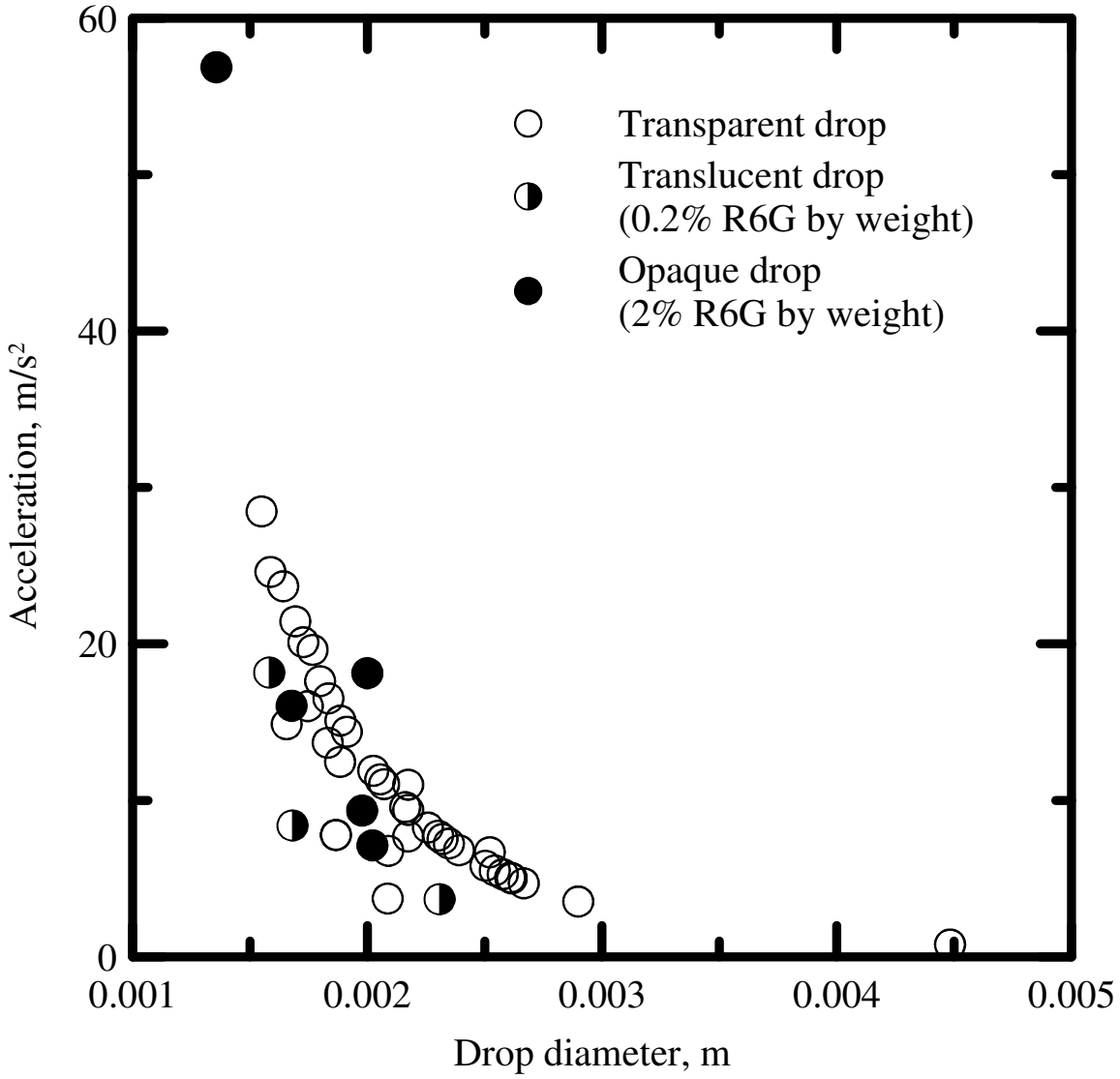

Fig. 3.7. Acceleration of drops based on the model. The data points that appear of the smooth curve are drops with identical absorptance and laser beam energy.

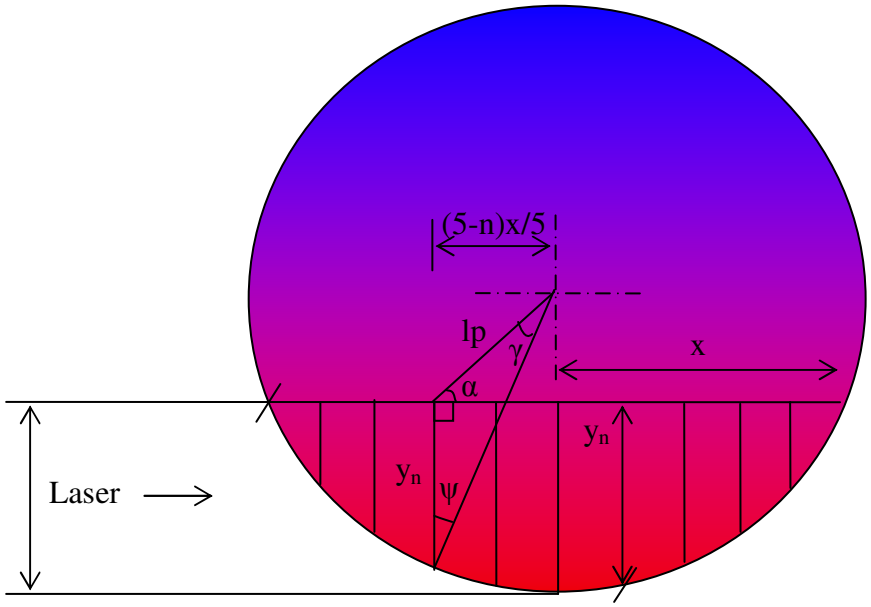

Fig. 3.8 Geometry of various parameters used in the model.

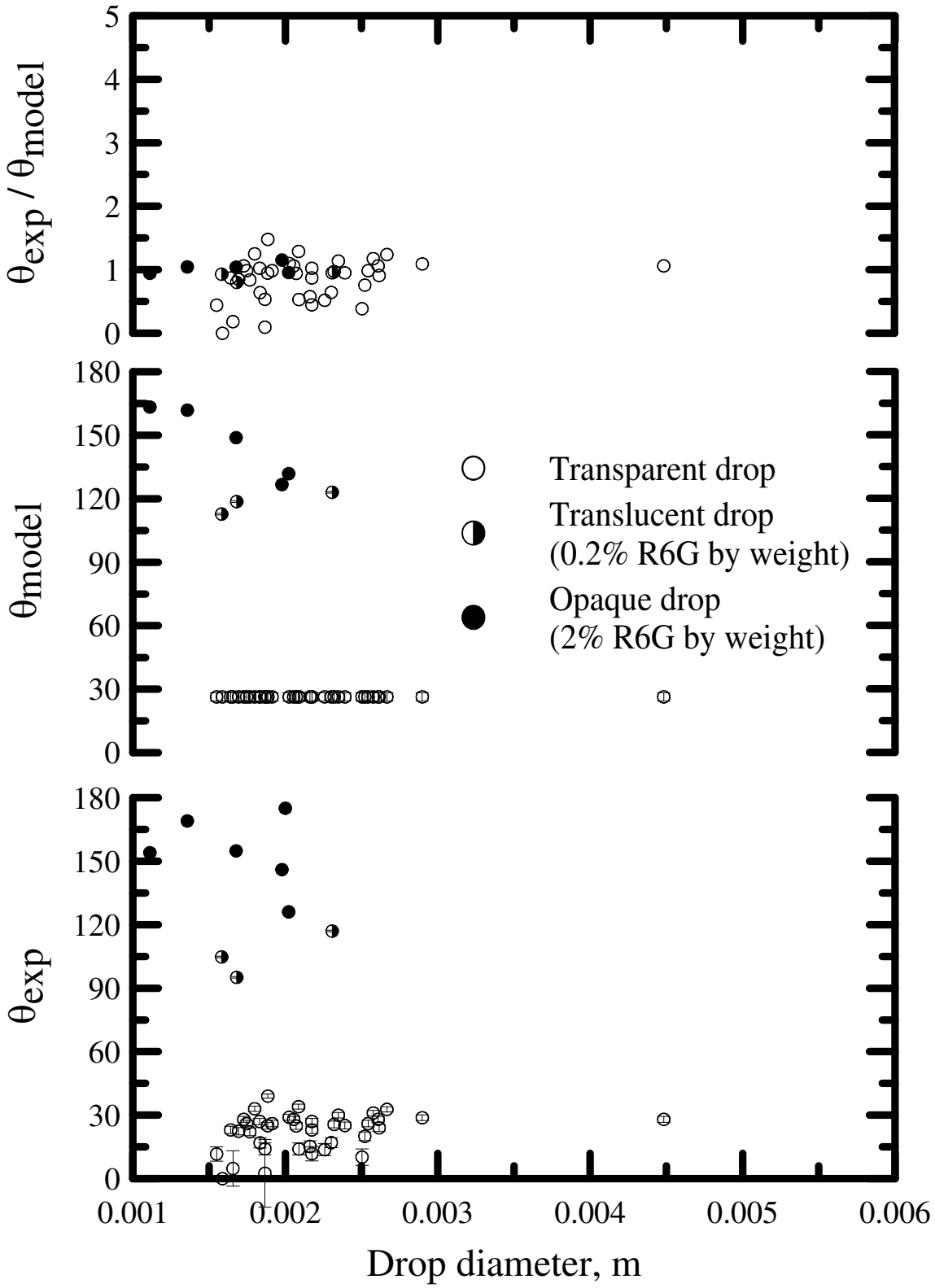

Fig. 3.9. The relation between the angles the drops moves, as observed and as predicted by the model.

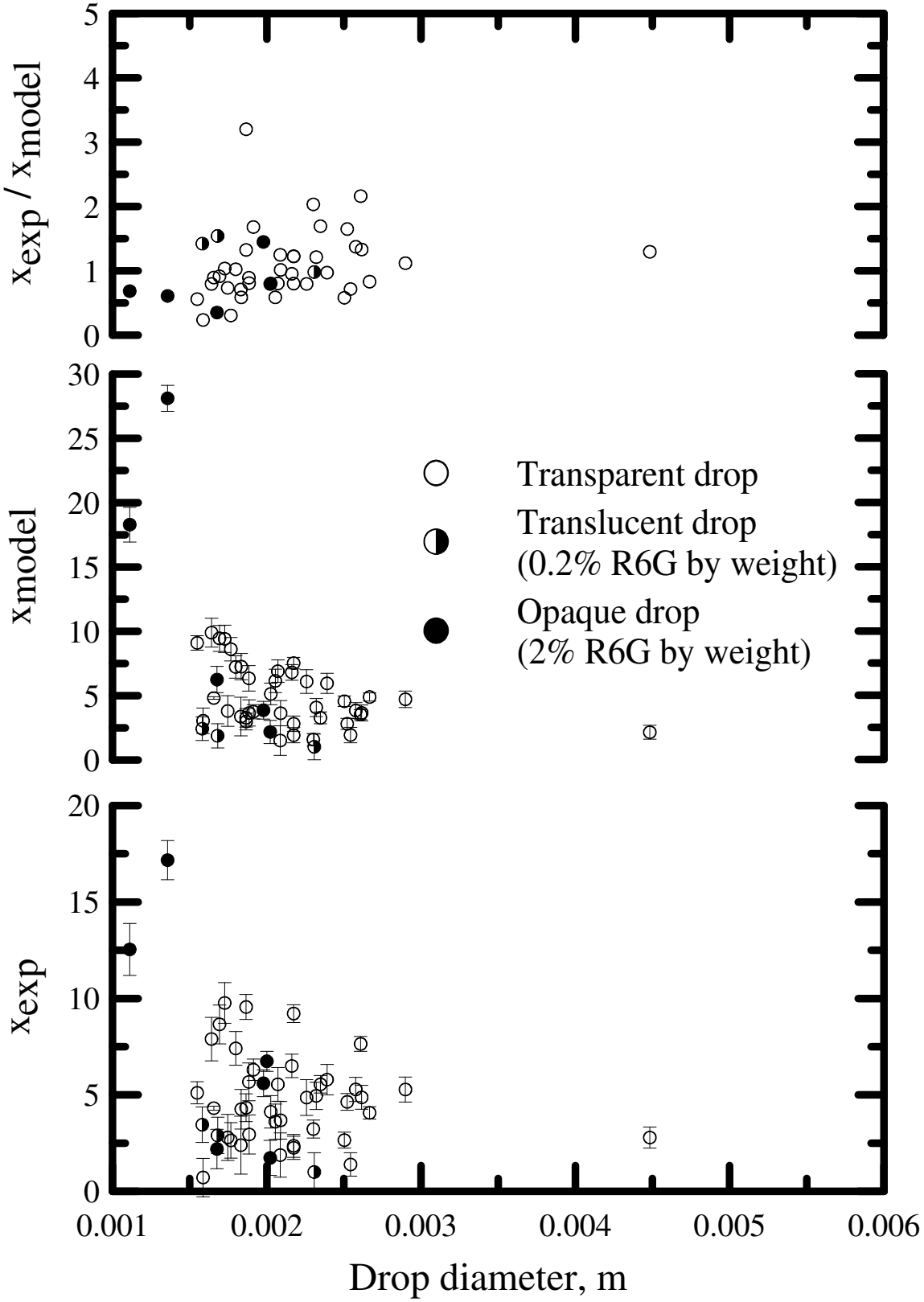

Fig. 3.10. The relation between the distance the drop moves, as observed and as predicted by the model.

CHAPTER IV

SUMMARY AND CONCLUSIONS

4.1 Summary

Drops of varying transparency (absorption coefficient, c_a ranging from $0.05m^{-1}$ to $6000m^{-1}$) and diameters (1mm – 4mm) were manipulated on a hydrophobic substrate, produced from Fluoropel® PFC M1604V coated glass slide, using Nd:YAG laser (532nm) pulsing at 10Hz, energy range of 3mJ – 12mJ per pulse. The motion of the drops was recorded and used to find drop kinematics and its dependence of drop size and beam energy. A phenomenological model was developed which explains the physics behind the observations and matches well with the observations.

4.2 Conclusions

The following conclusions can be drawn from the present study:

1. The angle at which the drops move depends upon the drop's transparency.
2. Transparent drops move toward the laser since the heating required for the motion comes primarily from the spark that is produced behind the drop due to the drop acting like a ball lens.

3. Dyed drops (translucent and opaque) move at large angles with the oncoming laser and the angle of motion depends on the drops' absorbance, resulting in higher angles for highly absorbent drops.
4. Based on the above, drops can be moved at any desired angle by varying the drops' absorbance and vice versa i.e. the drop's absorbance can be determined based on the angle at which it moves.
5. The distance moved by the drops is found to follow a log-normal distribution with average traveled distance of 5 drop diameters.
6. A model is developed which is a first for pulsed laser-induced drop motion and can predict the drop motion based on beam energy, drop diameter and absorption coefficient.
7. Higher velocities are reached, than observed by earlier researchers (Kotz et al., 2004; (Grigoriev et al., 2006), which can be used for quick response systems.

4.3 Future Work

The phenomenological model can be the first step toward automating laser-induced drop motion. The model can be improved by analyzing how the spark effects the motion i.e. how the plasma and the shock wave and the radiation heating from the spark influence drop motion for transparent drops. An infrared camera can be used to measure the temperature distribution on the surface of the drops. Other applications that can benefit from the present study include high energy laser propagation through the atmosphere which can be used for new laser-based systems being developed for wireless communication. The laser-induced spark has applications in internal combustion engines

where it offers various benefits over the conventional spark plug, research into this field can be undertaken to determine the feasibility of such a laser-based spark system.

Most of the present results can be characterized by the non-dimensional number $\sigma\rho d/\mu^2$ whose value for present experiments was found to mostly be 25000. Further study should explain the validity of the model at other values of this non-dimensional number.

REFERENCES

Alzuaga, S., J.-F. Manceau, et al. (2005). "Motion of droplets on solid surface using acoustic radiation pressure." Journal of Sound and Vibration **282**: 151-162.

Ashkin, A. (1987). "Optics: Laser manipulation of atoms." Nature (London) **330**(17): 608-609.

Astrakhan, I. M. (1960). "Pressure in a shock wave with intense spark discharge." U.S. Joint Publications Research Services **5867**: 1-9.

Ataide, C. H., F. A. R. Pereira, et al. (1999). "Wall effects on the terminal velocity of spherical particles in Newtonian and non-Newtonian fluids." Brazilian Journal of Chemical Engineering **16**(4).

Autric, M., P. Vigliano, et al. (1988). "Pulsed CO_2 Laser-Induced Effects on Water Droplets." AIAA Journal **26**(1): 65-71.

Beduneaua, J.-L. and Y. Ikeda (2004). "Spatial characterization of laser-induced sparks in air." Journal of Quantitative Spectroscopy & Radiative Transfer **84**: 123–139.

Bindhu, C. V., S. S. Harilal, et al. (1999). "Studies of nonlinear absorption and aggregation in aqueous solutions of rhodamine 6G using a transient thermal lens technique." Journal of Physics D: Applied Physics **32**: 407-411.

Bisyarin, B. P., V. V. Efremenko, et al. (1983). "Propagation of laser radiation in a water aerosol under aerosol breakup conditions." Soviet Physics Journal **26**(2): 121-140.

Carls, J. C. and J. R. Brock (1987). "Explosion of water droplet by pulsed laser heating." Aerosol science and technology **7**(1): 79-90.

Chen, S. H. (1999). "Thermocapillary Migration of a Fluid Sphere Parallel to an Insulated Plane." Langmuir **15**: 8618-8626.

Chen, S. H. (2000). "Movement of a Fluid Sphere in the Vicinity of a Flat Plane with Constant Temperature Gradient." Journal of Colloidal and Interface Science **230**: 157-170.

Chen, T.-H., Y.-J. Chuang, et al. (2007). "A wettability switchable surface by microscale surface morphology change." Journal of Micromechanics and Microengineering **17**: 489-495.

Cheow, L. F., L. Yobas, et al. (2007). "Digital microfluidics: Droplet based logic gates." Applied Physics Letters **90**: 054107-1-3.

Cho, S. K., H. Moon, et al. (2003). "Creating, Transporting, Cutting, and Merging Liquid Droplets by Electrowetting-Based Actuation for Digital Microfluidic Circuits." Journal of Microelectromechanical Systems **12**(1): 70-80.

Dholakia, K., G. Spalding, et al. (2002). Optical Tweezers: the next generation. Physics World**:** 31-35.

Dietzel, M. and D. Poulikakos (2005). "Laser-induced motion in nanoparticle suspension droplets on a surface." Physics of Fluids **17**: 102106-1-12.

Farahi, R. H., A. Passian, et al. (2004). "Microfluidic manipulation via Marangoni forces." Applied Physics Letters **85**(18): 4237-4239.

Farahi, R. H., A. Passian, et al. (2006). "Microscale Marangoni actuation: All-optical and all-electrical methods." Ultramicroscopy **106**: 815-821.

Ford, M. L. and A. Nadim (1994). "Thermocapillary migration of an attached drop on a solid surface." Physics of Fluids **6**(9): 3183-3185.

Fowler, J., H. Moon, et al. (2002). Enhancement of Mixing by Droplet-Based Microfluidics. IEEE**:** 97-100.

Garnier, N., R. O. Grigoriev, et al. (2003). "Optical Manipulation of Microscale Fluid Flow." Physical Review Letters **91**: 054501-054504.

Grigoriev, R. O., M. F. Schatz, et al. (2006). "Chaotic mixing in microdroplets." The Royal Society of Chemistry – Lab Chip **6**.

Hecht, E. (2001). Optics, Addison Wesley.

Incropera, F. P. and D. P. DeWitt (2002). Fundamentals of Heat and Mass Transfer, John Wiley & Sons.

Ivanov, E. V., V. Y. Korovin, et al. (1977). "Motion of optically dense liquid drops in a laser radiation field." Soviet Journal of Quantum Electronics **7(9)**: 1066-1071.

Karniakadis, G., A. Bestok, et al. (2001). Microflows and Nanoflows Fundamentals and Simulation, Springer.

Kitahata, H. (2006). "Spontaneous Motion of a Droplet Coupled with Chemical Reaction." Progress of Theoretical Physics Supplement **161**: 220-223.

Kotz, K. T., Y. Gu, et al. (2005). "Optically Addressed Droplet-Based Protein Assay." Journal of the American Chemical Society **127**: 5636-5637.

Kotz, K. T., K. A. Noble, et al. (2004). "Optical Microfluidics." Applied Physics Letters **85**: 2658-2660.

Moumen, N. (2006). Motion of a Drop on a Horizontal Solid Surface with Wettability Gradient. Department of Chemical and Biomolecular Engineering. Potsdam, NY, Clarkson University. **Ph. D., Chemical Engineering.**

Mushfique, H., J. Leach, et al. (2006). "An Optically Driven Pump for Microfluidics." SPIE **6326**(63260W).

Oh, S.-K., M. Nakagawa, et al. (2000). "Light-Guided Movement of a Liquid Droplet." Molecular crystals and liquid crystals science and technology. **345**: 311-316.

Ozen, O., N. Aubry, et al. (2006). "Monodisperse Drop Formation in Square Microchannels." Physical Review Letters **96**: 144501(4).

Park, B.-S. and R. L. Armstrong (1989). "Laser droplet heating: fast and slow heating regimes." Applied Optics **28**(17): 3671-3680.

Pegau, W. S., D. Gray, et al. (1997). "Absorption and attenuation of visible and near-infrared light in water: dependence on temperature and slinity." Applied Optics **36**(24): 6035-6046.

Phuoc, T. X. (2005). "An experimental and numerical study of laser-induced spark in air." Optics and Lasers in Engineering **43**: 113-129.

Phuoc, T. X. (2006). "Laser-induced spark ignition fundamental and applications." Optics and Lasers in Engineering **44**: 351-397.

Prishivalko, A. P. and S. T. Leiko (1984). "Effect of liquid surface layers on the heat release and heating of water droplets under the action of radiation " Soviet Physics Journal **5**(2): 301-303.

Rybalko, S., N. Magome, et al. (2004). "Forward and backward laser-guided motion of an oil droplet." Physical Review(E 70): 046301.

Scroll, R. D., R. Wunenberger, et al. (2007). "Liquid Transport due to Light Scattering." Physical Review Letters **98**(13): 133601(4).

Seeton, C. J. (2006). "Viscosity–temperature correlation for liquids." Tribology Letters **22**(1): 67-78.

Singh, P. I. and C. J. Knight (1978). Impulse Laser induced Shattering of Water Drops. AIAA.

Song, H., D. L. Chen, et al. (2006). "Reactions in Droplets in Microfluidic Channels." Angewandte Chemie International Edition **45**: 7336-7356.

Velev, O. D., B. G. Prevo, et al. (2003). "On-chip manipulation of free droplets." Nature **426**: 515-516.

White, F. M. (1991). Viscous Fluid Flow, McGraw-Hill, Inc.

Yang, J.-T., J. C. Chen, et al. (2004). "Droplet Manipulation on a Hydrophobic Textured Surface With Roughened Patterns." Journal of Microelectromechanical Systems **14**(3): 697-707.

Zakharin, B., J. Stricker, et al. (1999). "Laser-induced spark Schlieren imaging." AIAA Journal **37**(9): 1133-1135.

Zardecki, A. and J. D. Pendleton (1989). "Hydrodynamics of water droplets irradiated by a pulsed CO2 laser." Applied Optics **28**(3): 638-640.

Zhuzhukalo, E. V., A. N. Kolomifekii, et al. (1981). "Breakdown of atmospheric air by neodymium laser radiation forming large-diameter focusing spots." Kvantovaya Elektron. (Moscow) **8**(May): 1122-1123.

Zuev, V. E. and A. A. Zemlyanov (1983). "Explosion of a drop under the action of intense laser radiation." Soviet Physics Journal **26**(2): 149-159.

APPENDIX

Table A.1 Experimental Data

Clip name	Distance (pixels)	Distance (m)	Distance (drop dia.)	Angle (deg)
4_16_2007 2_55 PM_0001_01_07_8215	45	0.0039	1.9	34.0
4_16_2007 2_51 PM_0001_00_22_2390	94	0.0074	3.2	17.0
2_24_2007 6_39 PM_0001_02_29_7884	18	0.0011	0.7	0.0
4_16_2007 2_55 PM_0001_00_21_0532	59	0.0051	2.4	11.8
4_16_2007 2_51 PM_0001_00_37_9111	41	0.0035	1.4	26.0
4_12_2007 1_32 PM_0001_00_12_7191	42	0.0056	3.0	39.0
4_16_2007 2_55 PM_0001_00_23_4565	56	0.0049	2.3	23.0
4_16_2007 2_58 PM_0001_00_24_4989	139	0.0121	6.3	26.0
4_9_2007 10_32 PM_0001_00_23_4760	25	0.0044	2.4	27.0
4_16_2007 2_51 PM_0001_00_56_5401	134	0.0117	4.6	20.0
4_9_2007 11_51 PM_0001_01_03_1528	35	0.0049	2.8	26.0
4_16_2007 2_55 PM_0001_00_59_6195	150	0.0130	5.5	30.0
4_12_2007 1_17 PM_0001_08_49_8194	65	0.0084	4.1	29.0
4_12_2007 1_29 PM_0001_01_36_8707	90	0.0115	4.9	25.6
4_16_2007 2_55 PM_0001_00_48_0438	229	0.0199	7.6	28.0
2_24_2007 6_49 PM_0001_01_45_0323	172	0.0178	9.6	14.1
4_12_2007 1_17 PM_0001_10_49_8397	99	0.0127	4.9	24.0
2_24_2007 7_01 PM_0001_00_34_7784	60	0.0071	4.3	4.8
2_10_07_clip5 0 40 90_96	112	0.0079	5.1	11.7
4_12_2007 1_29 PM_0001_01_07_7999	106	0.0136	5.3	31.0
4_12_2007 1_38 PM_0001_01_02_8295	104	0.0133	7.4	33.0
2_24_2007 7_43 PM_0001_00_45_4955	55	0.0078	4.3	16.9
2_24_2007 6_49 PM_0001_01_45_9603	78	0.0081	4.3	2.5
4_12_2007 1_29 PM_0001_00_59_1428	54	0.0074	3.6	28.0
4_9_2007 11_15 PM_0001_00_43_6370	52	0.0077	3.7	14.0
2_24_2007 8_04 PM_0001_01_01_8995	90	0.0066	2.7	10.2
2_24_2007 7_19 PM_0001_00_54_5864	42	0.0096	5.4	22.2
4_16_2007 2_55 PM_0001_01_09_5872	230	0.0200	9.2	27.0
4_9_2007 11_09 PM_0001_00_57_3642	74	0.0107	5.7	25.0
4_9_2007 11_47 PM_0001_00_58_0310	80	0.0115	5.5	24.9
4_9_2007 11_18 PM_0001_01_04_8390	68	0.0110	4.9	13.7
4_9_2007 11_15 PM_0001_00_44_7278	87	0.0130	7.9	23.0
2_24_2007 7_39 PM_0001_01_46_8693	104	0.0147	8.7	22.4
2_10_07_1_3 55 23_29	163	0.0109	4.1	32.7
4_9_2007 11_18 PM_0001_00_48_9906	111	0.0169	9.8	28.0
4_9_2007 11_57 PM_0001_00_29_9609	73	0.0125	2.8	28.0
2_24_2007 7_19 PM_0001_00_57_7582	130	0.0140	6.5	15.2

Clip name	Distance (pixels)	Distance (m)	Distance (drop dia.)	Angle (deg)
2_24_2007 7_35 PM_0001_00_12_3946	93	0.0138	5.8	25.1
2_24_2007 7_32 PM_0001_00_26_9501	102	0.0153	5.3	28.8
4_9_2007 9_37 PM_0001_00_16_5063	52	0.0055	3.5	104.7
4_9_2007 9_37 PM_0001_00_27_6774	44	0.0049	2.9	95.1
4_16_2007 3_13 PM_0001_00_01_7488	21	0.0023	1.0	117.0
4_16_2007 3_12 PM_0001_00_14_3347	32	0.0035	1.7	126.0
4_16_2007 3_18 PM_0001_00_48_6585	101	0.0111	5.6	146.0
4_9_2007 10_10 PM_0001_00_09_1421	34	0.0037	2.2	154.9
4_16_2007 3_28 PM_0002_00_54_4255	113	0.0139	12.5	154.0
4_16_2007 3_28 PM_0001_00_49_3858	196	0.0233	17.2	169.0
4_16_2007 3_23 PM_0001_50_3245	155	0.0135	6.7	175.0

Table A.2 Experimental Data

Scale (5/10mm)	Drop dia (pixels)	Drop dia (m)	Drop mass (kg)	Velocity (m/s)	Velocity (dropdia/s)	Time (ms)	Beam Energy(mJ)
115	24	2.09E-03	4.76E-06	0.012	5.7	330	8
126	29	2.30E-03	6.38E-06	0.011	4.8	670	10
80	25	1.59E-03	2.09E-06	0.016	10.3	70	9.2
115	25	2.17E-03	5.38E-06	0.019	8.7	270	8
116	30	2.54E-03	8.61E-06	0.019	7.3	190	10
75	14	1.89E-03	3.51E-06	0.028	14.8	200	10
115	25	2.17E-03	5.38E-06	0.025	11.3	200	10
115	22	1.91E-03	3.67E-06	0.030	15.8	400	10
57	10	1.83E-03	3.22E-06	0.034	18.4	130	8
115	29	2.52E-03	8.40E-06	0.025	9.9	470	12
71	12	1.75E-03	2.79E-06	0.038	21.5	130	8
115	27	2.35E-03	6.78E-06	0.038	16.3	340	10
78	16	2.03E-03	4.35E-06	0.064	31.7	130	10
78	18	2.32E-03	6.54E-06	0.057	24.7	200	10
115	30	2.61E-03	9.30E-06	0.059	22.5	340	10
49	18	1.87E-03	3.40E-06	0.089	47.8	200	4.6
78	20	2.62E-03	9.37E-06	0.064	24.4	200	10
42	15	1.66E-03	2.38E-06	0.102	61.6	70	6.3
71	22	1.55E-03	1.95E-06	0.113	73.0	70	10
78	20	2.58E-03	8.96E-06	0.068	26.4	200	10
78	14	1.80E-03	3.05E-06	0.103	57.0	130	10
36	13	1.83E-03	3.23E-06	0.112	60.8	70	10
49	18	1.87E-03	3.40E-06	0.116	62.0	70	4.6
73	15	2.05E-03	4.54E-06	0.106	51.6	70	10
67	14	2.09E-03	4.78E-06	0.110	52.6	70	6

Scale (5/10mm)	Drop dia (pixels)	Drop dia (m)	Drop mass (kg)	Velocity (m/s)	Velocity (dropdia/s)	Time (ms)	Beam Energy(mJ)
69	34	2.50E-03	8.21E-06	0.095	37.9	70	10
44	16	1.77E-03	2.89E-06	0.137	77.7	70	10.6
115	25	2.17E-03	5.38E-06	0.143	65.8	140	12
69	13	1.88E-03	3.50E-06	0.178	94.5	60	8
70	15	2.07E-03	4.65E-06	0.164	79.2	70	10
62	14	2.26E-03	6.03E-06	0.157	69.5	70	10
67	11	1.64E-03	2.32E-06	0.216	131.5	60	10
36	12	1.69E-03	2.54E-06	0.209	123.7	70	10
75	40	2.67E-03	9.93E-06	0.155	58.2	70	10
66	11	1.73E-03	2.70E-06	0.241	139.5	70	10
58	26	4.48E-03	4.72E-05	0.096	21.5	130	10
47	20	2.16E-03	5.29E-06	0.201	92.8	70	10
34	16	2.39E-03	7.15E-06	0.198	82.7	70	10
34	19	2.90E-03	1.28E-05	0.219	75.4	70	10
95	15	1.58E-03	2.07E-06	0.042	26.6	130	12
91	15	1.68E-03	2.49E-06	0.070	41.4	70	6
91	21	2.31E-03	6.43E-06	0.017	7.2	140	6
91	18	2.02E-03	4.33E-06	0.025	12.4	140	7
91	18	1.98E-03	4.05E-06	0.055	28.0	200	10
91	15	1.68E-03	2.47E-06	0.053	31.4	70	6
81	9	1.11E-03	7.18E-07	0.107	96.5	130	10
84	11	1.36E-03	1.31E-06	0.117	85.8	200	10
115	23	2.00E-03	4.19E-06	0.104	51.9	130	10

Table A.3 Phenomenological model data

Surface Energy (J)	Kinetic Energy (J)	Fact (N)	Faero (N)	Fhys (N)	Final Temp. (K)	Re (-)	N.D. no. $\sigma\rho d/\mu^2$ (-)
1.38E-09	3.37E-10	1.77E-05	6.28E-09	9.57E-08	3.15E+02	1.49E+00	1.43E+04
4.41E-09	3.93E-10	4.94E-05	6.45E-09	1.06E-07	3.42E+02	1.54E+00	2.43E+04
4.09E-09	2.79E-10	5.15E-05	6.55E-09	7.28E-08	3.67E+02	1.56E+00	2.28E+04
3.52E-09	9.72E-10	4.14E-05	1.04E-08	9.97E-08	3.37E+02	2.49E+00	2.11E+04
4.40E-09	1.50E-09	4.75E-05	1.20E-08	1.17E-07	3.37E+02	2.86E+00	2.49E+04
4.43E-09	1.36E-09	5.30E-05	1.33E-08	8.65E-08	3.56E+02	3.15E+00	2.38E+04
4.42E-09	1.62E-09	5.05E-05	1.35E-08	9.97E-08	3.46E+02	3.21E+00	2.41E+04
4.43E-09	1.67E-09	5.27E-05	1.46E-08	8.78E-08	3.55E+02	3.47E+00	2.38E+04
3.53E-09	1.83E-09	4.40E-05	1.56E-08	8.40E-08	3.47E+02	3.72E+00	2.05E+04
5.30E-09	2.60E-09	5.61E-05	1.59E-08	1.16E-07	3.45E+02	3.77E+00	2.76E+04
3.54E-09	1.97E-09	4.47E-05	1.66E-08	8.01E-08	3.50E+02	3.95E+00	2.05E+04
4.41E-09	4.97E-09	4.90E-05	2.27E-08	1.08E-07	3.41E+02	5.41E+00	2.44E+04

Surface Energy (J)	Kinetic Energy (J)	Fact (N)	Faero (N)	Fhys (N)	Final Temp. (K)	Re (-)	N.D. no. $\sigma\rho d/\mu^2$ (-)
4.42E-09	8.99E-09	5.18E-05	3.29E-08	9.29E-08	3.50E+02	7.83E+00	2.39E+04
4.41E-09	1.08E-08	4.93E-05	3.37E-08	1.06E-07	3.42E+02	8.01E+00	2.43E+04
4.40E-09	1.60E-08	4.70E-05	3.87E-08	1.20E-07	3.36E+02	9.20E+00	2.51E+04
2.02E-09	1.35E-08	2.65E-05	4.20E-08	8.56E-08	3.26E+02	1.00E+01	1.54E+04
4.40E-09	1.90E-08	4.70E-05	4.21E-08	1.20E-07	3.36E+02	1.00E+01	2.51E+04
2.66E-09	1.24E-08	3.54E-05	4.27E-08	7.60E-08	3.41E+02	1.02E+01	1.72E+04
4.46E-09	1.24E-08	5.54E-05	4.43E-08	7.11E-08	3.76E+02	1.05E+01	2.44E+04
4.40E-09	2.08E-08	4.73E-05	4.43E-08	1.18E-07	3.36E+02	1.06E+01	2.50E+04
4.44E-09	1.60E-08	5.37E-05	4.66E-08	8.25E-08	3.60E+02	1.11E+01	2.38E+04
4.43E-09	2.01E-08	5.34E-05	5.17E-08	8.42E-08	3.58E+02	1.23E+01	2.38E+04
2.02E-09	2.27E-08	2.65E-05	5.45E-08	8.56E-08	3.26E+02	1.30E+01	1.54E+04
4.42E-09	2.56E-08	5.15E-05	5.51E-08	9.43E-08	3.49E+02	1.31E+01	2.39E+04
2.64E-09	2.89E-08	3.23E-05	5.81E-08	9.59E-08	3.29E+02	1.38E+01	1.81E+04
4.41E-09	3.70E-08	4.78E-05	6.01E-08	1.15E-07	3.38E+02	1.43E+01	2.48E+04
4.71E-09	2.72E-08	5.67E-05	6.13E-08	8.11E-08	3.65E+02	1.46E+01	2.49E+04
5.31E-09	5.51E-08	5.92E-05	7.86E-08	9.97E-08	3.55E+02	1.87E+01	2.71E+04
3.53E-09	5.55E-08	4.36E-05	8.48E-08	8.64E-08	3.45E+02	2.02E+01	2.06E+04
4.42E-09	6.27E-08	5.14E-05	8.59E-08	9.50E-08	3.49E+02	2.04E+01	2.39E+04
4.41E-09	7.41E-08	4.98E-05	8.95E-08	1.04E-07	3.43E+02	2.13E+01	2.42E+04
4.45E-09	5.40E-08	5.49E-05	8.96E-08	7.53E-08	3.69E+02	2.13E+01	2.41E+04
4.44E-09	5.57E-08	5.45E-05	8.96E-08	7.77E-08	3.66E+02	2.13E+01	2.40E+04
4.40E-09	1.19E-07	4.66E-05	1.05E-07	1.22E-07	3.35E+02	2.49E+01	2.53E+04
4.44E-09	7.83E-08	5.43E-05	1.05E-07	7.92E-08	3.64E+02	2.50E+01	2.39E+04
4.38E-09	2.18E-07	3.69E-05	1.09E-07	2.06E-07	3.19E+02	2.60E+01	3.25E+04
4.42E-09	1.07E-07	5.06E-05	1.10E-07	9.92E-08	3.46E+02	2.61E+01	2.40E+04
4.41E-09	1.40E-07	4.87E-05	1.20E-07	1.10E-07	3.40E+02	2.84E+01	2.45E+04
4.40E-09	3.05E-07	4.50E-05	1.60E-07	1.33E-07	3.31E+02	3.81E+01	2.60E+04
2.31E-09	1.83E-09	3.77E-05	1.68E-08	9.33E-08	3.48E+02	4.00E+00	1.81E+04
1.48E-09	6.04E-09	2.09E-05	2.96E-08	9.92E-08	3.25E+02	7.05E+00	1.37E+04
2.78E-09	8.82E-10	2.37E-05	9.66E-09	1.36E-07	3.27E+02	2.30E+00	1.94E+04
3.85E-09	1.36E-09	3.08E-05	1.28E-08	1.19E-07	3.44E+02	3.05E+00	2.19E+04
4.22E-09	6.22E-09	3.79E-05	2.77E-08	1.17E-07	3.50E+02	6.59E+00	2.33E+04
5.66E-09	3.43E-09	3.96E-05	2.23E-08	9.89E-08	3.88E+02	5.31E+00	2.97E+04
7.01E-09	4.13E-09	6.96E-05	3.01E-08	6.55E-08	5.11E+02	7.16E+00	4.23E+04
1.35E-08	8.88E-09	7.44E-05	4.00E-08	8.00E-08	5.81E+02	9.51E+00	6.60E+04
5.44E-08	2.25E-08	7.59E-05	5.24E-08	1.18E-07	1.05E+03	1.25E+01	1.89E+05

Table A.4 Phenomenological model data and comparison with experiments

Absorptance (-)	No. of cells penetrated	Dist. Moved model, xt (m)	Angle model, at (deg)	xe/xt (-)	ae/at (-)	Change in density (heated region), Deltarho (kg/m^3)	Instantaneous start acceleration (m/s^2)
2.38E-04	10	1.23E-03	26.39	3.18	1.29	4.57	3.72
2.59E-04	10	3.65E-03	26.39	2.03	0.64	12.62	7.74
1.81E-04	10	4.83E-03	26.39	0.24	0.00	20.01	24.60
2.47E-04	10	4.18E-03	26.39	1.23	0.45	10.92	7.69
2.80E-04	10	4.94E-03	26.39	0.72	0.99	11.05	5.52
2.17E-04	10	6.88E-03	26.39	0.81	1.48	16.71	15.09
2.47E-04	10	6.11E-03	26.39	0.80	0.87	13.64	9.39
2.20E-04	10	7.17E-03	26.39	1.68	0.99	16.35	14.38
2.11E-04	10	6.17E-03	26.39	0.71	1.02	13.95	13.68
2.78E-04	10	7.09E-03	26.39	1.65	0.76	13.41	6.68
2.01E-04	10	6.64E-03	26.39	0.73	0.99	14.99	16.02
2.63E-04	10	7.68E-03	26.39	1.69	1.14	12.29	7.24
2.32E-04	10	1.04E-02	26.39	0.80	1.10	15.06	11.89
2.60E-04	10	9.46E-03	26.39	1.21	0.97	12.48	7.53
2.86E-04	10	9.22E-03	26.39	2.16	1.06	10.69	5.06
2.15E-04	10	5.57E-03	26.39	3.20	0.53	7.80	7.79
2.86E-04	10	9.57E-03	26.39	1.33	0.91	10.65	5.01
1.90E-04	10	7.98E-03	26.39	0.90	0.18	12.26	14.87
1.76E-04	10	1.41E-02	26.39	0.56	0.44	22.62	28.47
2.83E-04	10	9.90E-03	26.39	1.37	1.17	10.86	5.27
2.07E-04	10	1.30E-02	26.39	1.02	1.25	17.92	17.62
2.11E-04	10	1.33E-02	26.39	0.59	0.64	17.40	16.52
2.15E-04	10	6.10E-03	26.39	1.33	0.09	7.80	7.79
2.35E-04	10	1.26E-02	26.39	0.59	1.06	14.76	11.34
2.38E-04	10	7.59E-03	26.39	1.01	0.53	8.65	6.77
2.77E-04	10	1.14E-02	26.39	0.58	0.39	11.28	5.82
2.03E-04	10	1.52E-02	26.39	0.63	0.84	19.51	19.62
2.47E-04	10	1.64E-02	26.39	1.22	1.02	16.37	11.00
2.17E-04	10	1.20E-02	26.39	0.89	0.95	13.38	12.46
2.36E-04	10	1.43E-02	26.39	0.80	0.94	14.59	11.04
2.55E-04	10	1.38E-02	26.39	0.80	0.52	12.95	8.26
1.88E-04	10	1.63E-02	26.39	0.80	0.87	20.61	23.69
1.95E-04	10	1.60E-02	26.39	0.92	0.85	19.64	21.44
2.90E-04	10	1.30E-02	26.39	0.83	1.24	10.39	4.69
1.99E-04	10	1.63E-02	26.39	1.04	1.06	19.05	20.11
4.13E-04	10	9.65E-03	26.39	1.30	1.06	5.53	0.78

Absorptance (-)	No. of cells penetrated	Dist. Moved model, xt (m)	Angle model, at (deg)	xe/xt (-)	ae/at (-)	Change in density (heated region), Deltarho (kg/m^3)	Instantaneous start acceleration (m/s^2)
2.45E-04	10	1.47E-02	26.39	0.95	0.58	13.75	9.57
2.67E-04	10	1.42E-02	26.39	0.97	0.95	11.99	6.81
3.09E-04	10	1.37E-02	26.39	1.12	1.09	9.34	3.53
9.33E-01	9	3.84E-03	112.75	1.42	0.93	14.35	18.17
9.45E-01	8	3.16E-03	118.64	1.54	0.80	7.48	8.39
9.80E-01	6	2.36E-03	123.02	0.98	0.95	8.10	3.68
9.90E-01	5	4.40E-03	131.85	0.80	0.96	13.17	7.12
9.89E-01	6	7.64E-03	126.67	1.45	1.15	15.05	9.34
1.00E+00	3	1.05E-02	148.85	0.35	1.04	26.22	16.04
1.00E+00	3	2.03E-02	163.30	0.69	0.94	63.04	96.96
1.00E+00	2	3.82E-02	161.80	0.61	1.04	83.92	56.87
1.00E+00	1	1.31E-01	158.50	0.10	1.10	222.84	18.13

VITA

Rohit Shukla

Candidate for the Degree of

Master of Science

Thesis: EFFECT OF LIQUID TRANSPARENCY ON LASER-INDUCED MOTION OF DROPS

Major Field: Mechanical Engineering

Biographical:

Personal Data: Born in Dehra Doon on 1st December, 1983. Son of Dr. Daya Shankar Shukla and Mrs. Promila Shukla.

Education: Completed Bachelor of Engineering from Mumbai University, Mumbai, India in July 2005. Completed the requirements for the Master of Science in Mechanical Engineering at Oklahoma State University, Stillwater, Oklahoma in July, 2007.

Experience: Worked as a trainee engineer on refrigeration units at Godrej India Ltd. Employed by MAE, OSU as teaching assistant for Engineering Dynamics, Experimental Fluid Dynamics and Computer Methods. Served as a tutor for the CEAT Academic Excellence Center for Physics and Math.

Name: Rohit Shukla Date of Degree: December, 2007

Institution: Oklahoma State University Location: Stillwater, Oklahoma

Title of Study: EFFECT OF LIQUID TRANSPARENCY ON LASER-INDUCED MOTION OF DROPS

Pages in Study: 70 Candidate for the Degree of Master of Science

Major Field: Mechanical Engineering

Scope and Method of Study: An experimental study of laser-induced drop motion and the effect of drop transparency on the motion of drops is described here. Drops of varying transparency and size (1mm – 4mm) can be manipulated on a hydrophobic substrate, which is easily produced from a commercially available coating, using Nd:YAG laser (532nm) pulsing at 10Hz in the energy range of 3mJ – 12 mJ. The results of the present study should have wide applications. The main beneficiaries of the study are field of fluidics - fluid manipulation especially for bio and chemical applications, laser propagation through drops and laser-induced spark for automotive ignition systems where it offers various benefits over the conventional spark plug.

Findings and Conclusions: The main conclusions are - The angle at which the movement occurs depends upon the drop transparency. Transparent drops move toward the laser beam at small angles with it, translucent drops move almost normal to the laser beam and opaque drops move along the laser at large angles away from it.
A phenomenological model was developed and validated, which explains the physics behind the observations. The model showed good agreement with experimental observations.

ADVISER'S APPROVAL: Dr. K. A. Sallam